Air solar flat plate collector analysis with induced turbulence

A Dissertation submitted
in partial fulfillment of the requirements for
the degree of

Master of Engineering

in

Thermal Engineering

by

Gagandeep Singh Bagga

Registration No.: 801483009

Under the Supervision of

Dr. V.P. Agrawal
(Visiting Professor)
(MED)

Sandeep Kumar
(Visiting Assistant Professor)
(MED)

MECHANICAL ENGINEERING DEPARTMENT

THAPAR UNIVERSITY, PATIALA

July, 2016

CERTIFICATE

I hereby declare that the thesis entitled "**Air solar flat plate collector analysis with induced turbulence**" is an authentic record of my work carried out as requirements for the award of the degree of **Master of Engineering** in **Thermal Engineering** at **Thapar University, Patiala** under the supervision of **Dr. V. P. Agrawal**, Visiting Professor, **Sandeep Kumar**, Visiting Assistant Professor, MED, Thapar University, Patiala during July, 2014 to July, 2016. No part of the matter embodied in this report has been submitted to any other university or institute for the award of any degree.

Date: Patiala (15/07/2016)

Place: Patiala

Gagandeep Singh Bagga

801483009

It is certified that the above statement made by the student is correct to the best of my/our knowledge and belief.

Dr. V.P. Agrawal

MED, Thapar University,

Patiala – 147004.

Sandeep Kumar

MED, Thapar University,

Patiala – 147004.

Countersigned by

Dr. S.K. Mohapatra

Head, Mechanical Engineering Department,

Thapar University, Patiala – 147004.

Dean of Academic Affairs

Thapar University, Patiala – 147004.

Dedicated to My Teacher

Dr. Vijender Singh

&

My Parents

Varinder Singh Bagga

Nirmal Kaur

Acknowledgements

I would like to devote my deepest gratitude to my supervisor, **Dr. V.P.Agrawal**, for his encouraging guidance, goading, patience, and countless number of discussions on problem tackling. Your advice has helped me to thwart many problems on the embarking journey to research. The opportunity, support, exposure and atmosphere provided by the Thapar University, Patiala, to carry out my studies are appreciated.

I am always in debt to my Co-guide **Sandeep Kumar** for giving me all the help I needed in every critical as well pivotal moment. The voluminous difference between books and practical knowledge has been bridged only because of his industrious and indefatigable hold to this project. The ineffable help has engendered such experimental set-up.

My respect goes to **Mr.Gurpinder Singh** (PhD Student, MED, Thapar University) for helping in every possible way to tackle the pragmatic problems on my embarking journey to fabrication of set-up.

The authors whose work has been consulted, I am obliged. I want to extend my gratitude to all those who helped me in this project.

I pay my sincere respect to my parents and my friends for helping me whenever I asked. Their unconditional love and selfless attitude has helped me a lot to brave all the adversaries and adversities.

Gagandeep Singh Bagga

801483009

Abstract

industrial energy requirement is the solar air heater to pre-heat air for further drying, heating, lithe delicate parts and many more purposes. The solar air heaters performance rely on (Lauva et al. 2006; Palabinskis et al. 2008), passage given to air flow as single pass or double pass air flow or multi-pass flow (Forson, Nazha, and Rajakaruna. 2003) and weather conditions. This report ponders over the various design parameters considered while designing the experimental set-up along with the effects of these parameters on performance of solar air collector. Two different convection modes were analysed namely; Natural mode and Forced convection mode to contemplate over the heat transfer coefficient associated with each case. Double glass as top cover is used to minimize losses pertaining to radiation. To reduce shading losses glass itself is used to make air flow through multi passes. CFD modelling is applied to predict the temperature pattern of air with radiation model DTRM and k-ε̇ turbulence model. The setup works at an atmospheric pressure of 1.013N/m^2. The modelling gives good results when compared experimentally with natural convection mode. The temperature characteristics of air are plotted in the report comparing it with both convection modes. Artificial roughening of absorber unit is crucial to increasing heat transfer rates to air (Anil singh Yadav et al. 2014) and is done in the passages taken by air. Twisted wires is used which would set the air in the vicinity into circular motion analogous to swirling of fuel in internal combustion engines. It has been found that number of passages increases residence time of air and heat transfer to air, although increases pressure loss. The shading losses are compensated with glass partitions. Peak efficiencies are achieved on a sunny day from 12 noon to 2 pm.

Keywords: Solar collector; Double glass cover; Turbulence; CFD modelling; Solar drying.

Contents

List of Figures

List of Tables

Nomenclature

C_p:	Specific heat of air (J/kg K)
D:	Equivalent or hydraulic diameter of duct (mm)
e:	Rib height (mm)
H:	Depth of duct (mm)
h:	Heat transfer coefficient ($W/m^2.K$)
I_b:	Intensity of solar radiation (W/m^2)
k:	Thermal conductivity of air (W/m.K)
m:	Mass flow rate (kg/s)
P	Pitch (mm)
P_m	Mechanical energy consumed for propelling air through collector (Watts)
Q_u	Useful heat gain (W/m^2)
Ta	Ambient temperature (K)
To	Air temperature at exit (K)
W	Width of duct (mm)
w	Width of rib (mm)
ΔP	Pressure drop (Pa)
$\overline{Nu}$	Average nusselt number
$\overline{f}$	Average friction factor
$\overline{St}$	Average Stanton number
e/D	Relative roughness height
e/H	Rib to channel height ratio
e^+	Roughness Reynold number

P/e	Relative roughness pitch
Pr	Prandtl number
~	Angle of attack, degree
¤	Wedge angle/chamfer angle, degree

Chapter 1

Introduction & Objectives

1.1 Introduction

Most basic Form of application of sun is the of Solar Air Heating collector because of its simplicity in construction, Eco-Friendly, Wide usage particularly in Grain Drying Field. Radiations from sun in form of heat are accumulated and the heat is transferred to the fluid (water/Air). Solar collectors may be Active or Passive solar heating Systems. The most economic, environment friendly use of such rustic device is the drying of spices, fruits, vegetables, and crops to preserve them for longer period of time. The moisture content retained by a crop, fruit or vegetable plays a crucial role in deciding the time before it starts to addle. Solar collectors are easy to use and easy to construct and could be made of any size corresponding to the amount of crops, fruits or vegetables to be dried. The size of solar air heater bears direct relation with the mass flow of air required at collector exit at specific temperature.

1.2 Solar Air Heaters categorization

The Major categorization of solar collector are the single pass with Front and back duct and the Double pass Double duct.

- Flat Plate collectors with Temperature of fluid not rising above 80^{o}C.
- Concentrating Collectors with Temperature of fluid going above 140^{o}C.

Rhushi Prasad, Byregowda and Gangavati (2010) categorized collectors as:-

- Hydronic Collectors- Water as Heat Transfer Fluid.
- Air Collectors- Air as heat transfer Fluid.

1.3 Conventional Air Heater

The conventional air heaters comprises of opaque Black Board (Dull) color painted absorber plate, Glass cover, Air duct, Bottom plate and Insulation. They are simple to construct and many times the absorber plate may be of irregular shape to increase heat transfer to air.

The major cons to solar air heaters is the copious amount of air to be dealt with leading to significant power consumptions if pressure drop is not monitored. Cost associated increases profusively upon selection material of absorber plate.

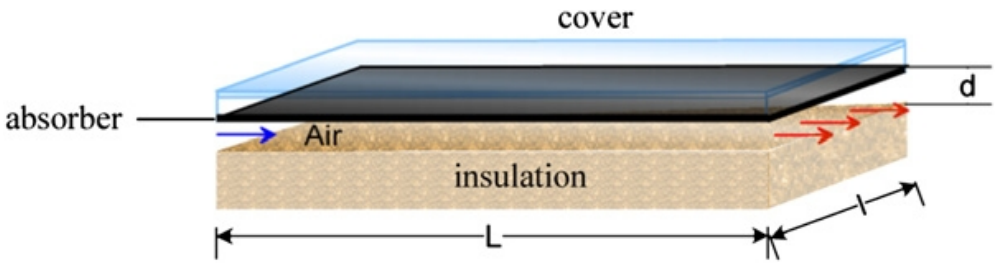

Fig 1.1: Conventional Air Heater[1].

1.3.1 Variation of conventional Solar Heater

Two Pass Solar Air Heater: - The radiation losses from top are reduced with this methodology. An estimated increase of 5 to 10 % is observed. The air 1st receives energy by flowing in between the glass covers then after preheating it flows between absorber and bottom plate.

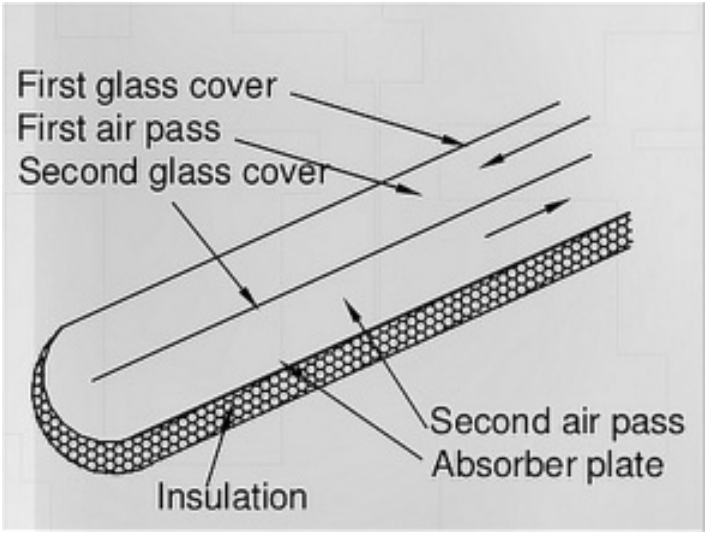

Fig 1.2: Two pass Air Heater[2].

[1] https://www.researchgate.net/figure/241093823_fig1_Fig-3-Sketch-of-a-conventional-solar-air-heater.

1.4 New Designs of Solar Air Heaters

Novel designs improves solar collector efficiency because of they entertain large flow contrary to less drop in pressure. Usually the absorbing surface is porous. Pressure drop is less if flow is maintained uniform. In some cases it has been found that pressure loss is **200 times** less than conventional air heaters leading to huge savings in power consumption.

The solar radiation is incidented on porous absorber through which air flows thus providing large area to air flow thereby increasing heat transfer to air.

1.4.1 Matrix Solar Air H

Usually these type heaters involve twisted porous absorber section which transfers the heat energy to the air. Performance is high besides higher flow rates.

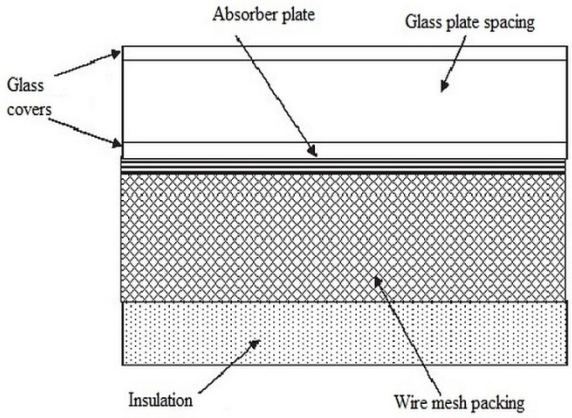

Fig 1.3: Matrix Solar air Heater[3].

1.4.2 Plastic Solar Air Heater

To deal with copious supply of air these types of air heaters comes in picture. They inflate and take the specific shape as air is passed through them. Absorber is dull shade of black color painted polyester sheet cringed at edges of PVC (poly vinyl chloride) sheets and is shrouded by the PVC. Efficiencies can up to 68% is achieved by researchers. These types of solar air heaters can be extended up to 50 meters in length and can handle mass flow of 5 kg/s.

---

[2] http://stonehavenlife.com/comparing-solar-air-heater-designs-performance/

[3] M.K. LALJI & R.M. SARVIYA (2011), Experimental Investigations on Packed Bed Solar Air Heater, *Current World Environment, Vol. 6(1), 151-157.*

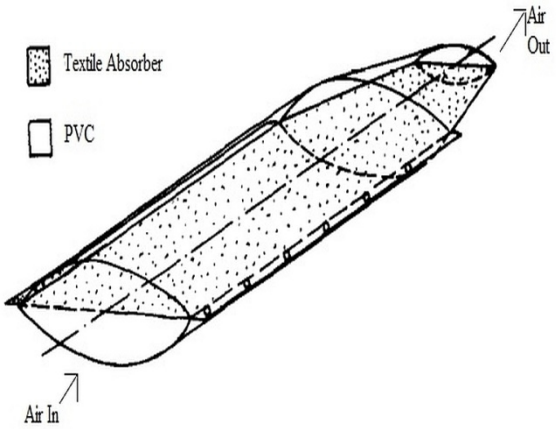

Fig 1.4: Plastic Solar air Heater[4].

1.5 Unglazed Transpired Solar Air Heater

They are Quotidian in cold countries for room heating purposes. They comprise a black color painted absorber which transfers heat to air when air flows over it after sucked in through porous sheet. The porosity index of such heaters ranges 0.5 %. In northern countries this type of collector is vertically oriented. Nowadays polyethylene or styrene is used as low conductivity materials to cut the cost associated with it. In order to forbid reverse flow in the top section minimum velocity is kept 1.25 m/s.

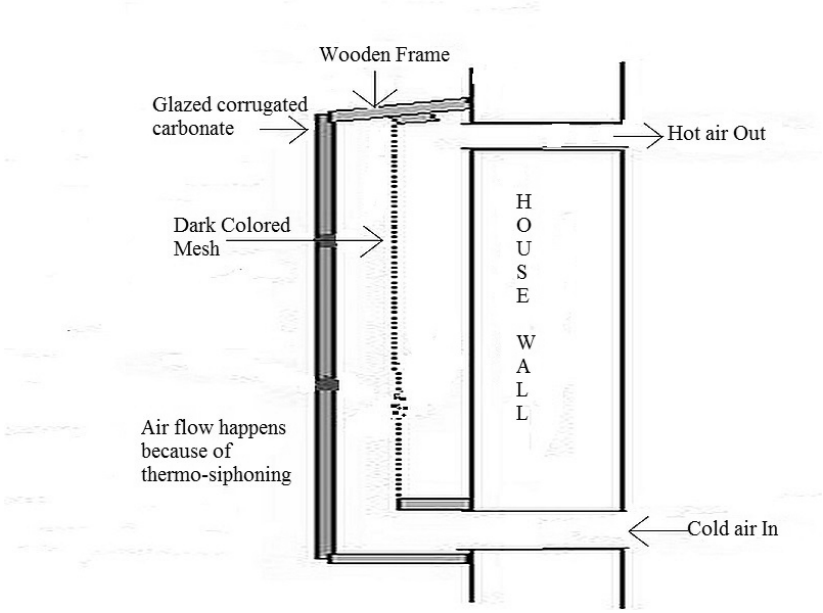

Fig 1.5: Closed system Transpired solar air Heater[5].

[4] □ □□□ □□□ □□□□□□□□□□□□□r □□□r □□□□□r □□□□c □□□□□□□□□□d □□□□*Renew Energy*, vol. 16, no. 1□4, pp. 618□623, 1999.
[5] http://rimstar.org/renewnrg/solarair.htm

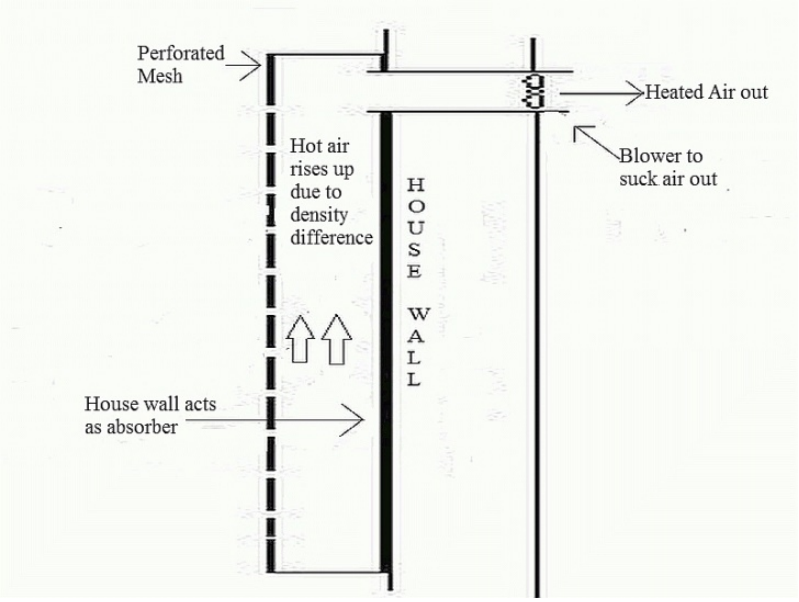

Fig 1.6: Open System Transpired Solar Air heater[6].

1.6 Flat plate Solar Air Heater Efficiency

Lauva et al. 2006; Palabinskis et al. 2008 deduced that efficiency of Solar Flat Plate collector depends upon these factors:-

- Absorber Material of plate
- Covered material
- Air velocity in collector
- Air Temperature growth further depend upon (Wind, Clouds, Ambient air temperature etc.
- Thermo-hydraulic efficiency.
- Roughness/turbulence introduced with aid of external body.

[6] http://rimstar.org/renewnrg/solarair.htm

1.7 Open sun drying

The applications of Solar air Heaters are:-

- Crops Drying
- Waste food Processing
- Lithe Delicate plastic parts
- Spices drying
- Fruits drying
- Room Heating
- Pre-Heating of Air

Open sun drying is the simplest type of drying which has been in use in Indian grain markets. The crops are winnowed and scattered on floor and sun rays are allowed to fall on them. Some rays get absorbed and some get reflected.

Advantages: - Ease of operation, Almost bears no cost, Easy loading on trolleys.
Disadvantages: - Depends on mercy of weather, Moisture cannot be controlled, Drying time is enormous.

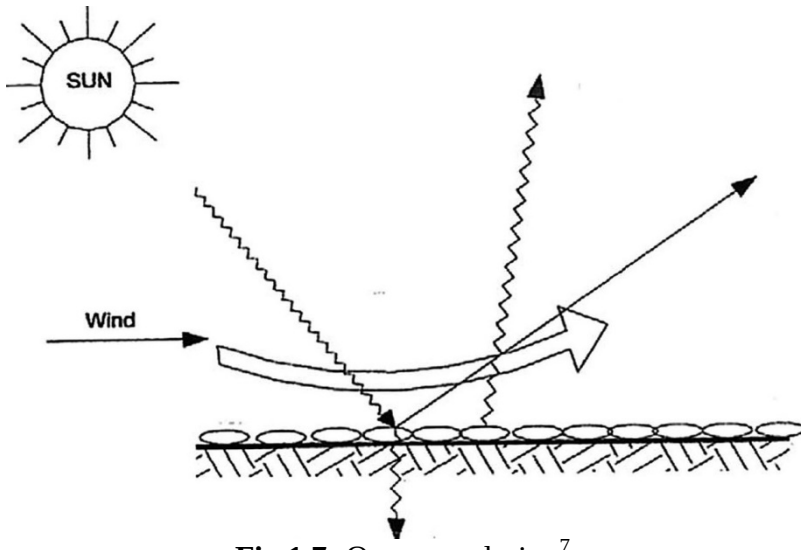

Fig 1.7: Open sun drying[7]

[7] Prakash, O. and Kumar, A. Historical Review and Recent Trends in Solar Drying Systems. *International Journal of Green Energy 10*, 7 (2013), 690□738.

1.7.1 Indirect drying

To reduce or even eradicate discoloration and surface cracks crops are given indirect exposure

of Sun-rays. Sun-rays penetrate through a glass cover and heats up the stuff to be dried.

This method has advantage over contamination and as well blow away problems.

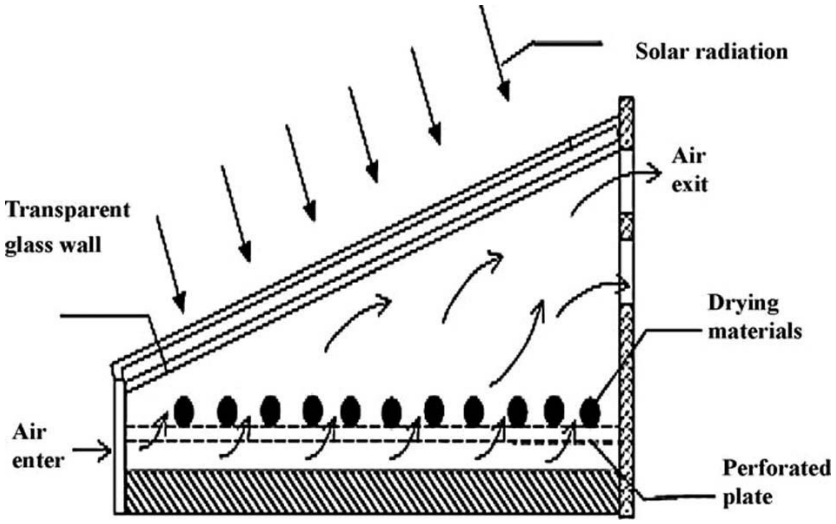

Fig 1.8: Passive solar food dryer[8]

1.7.2 Solar air Heater for processing Waste food

Solar heater used to dry food waste in order to feed it to the animals 1st surfaced in 1998. Much of the waste was fed and some was converted to decomposed food as urea to plants.

[8] Renewable and Sustainable Energy Reviews, 13(6-7), Sharma et al., Solar-energy drying systems: A review, pp. 1185□1210, 2009.

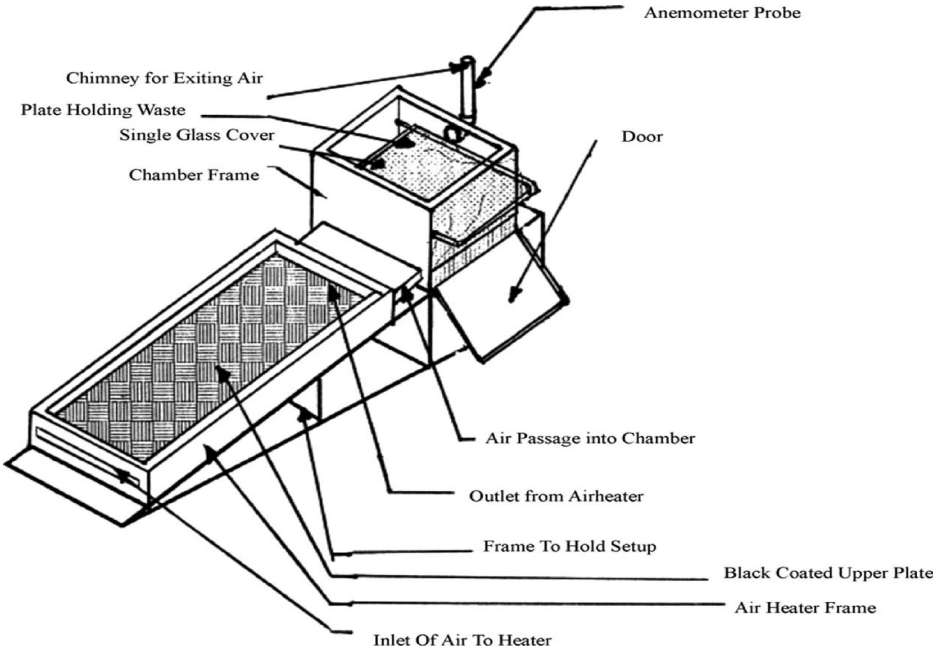

Fig 1.9: Processing of waste food[9]

1.7.3 Copra drying

Coconut meat is extracted from coconuts with copra drying. The main purpose behind it copra drying is to concentrate coconut oil content. Moisture is reduced from 60 % to 8 % generally. India produces 14.5 billion units of coconut which are used for cooking oil and making ropes in India. It takes 7 coconuts to make 1kg of copra.

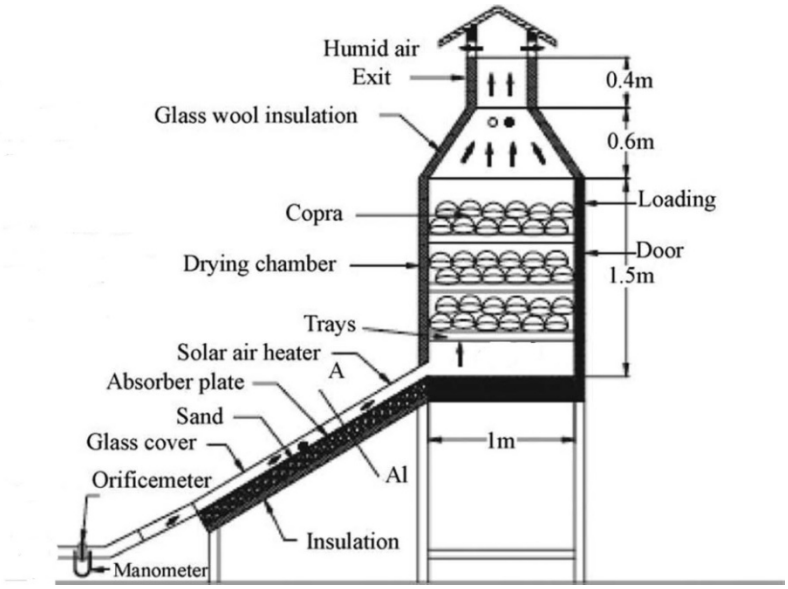

Fig 1.10: Copra Dryer[10]

[9] Nijmeh et al., Design and testing of solar dryers for processing food wastes, *Thermal Engineering*, 18(12), pp. 1337□1346, 1998.

1.7.4 Solar Air heater for Spices drying

This conventional type solar collector used solar arrays to heat up air and then pass it through mustard powder for its moisture reduction. For longer storage it is a very decisive factor. Too higher the moisture reduction rate it will crack the surface of crop. Apposite moisture removal rate is key to avoid addling issues.

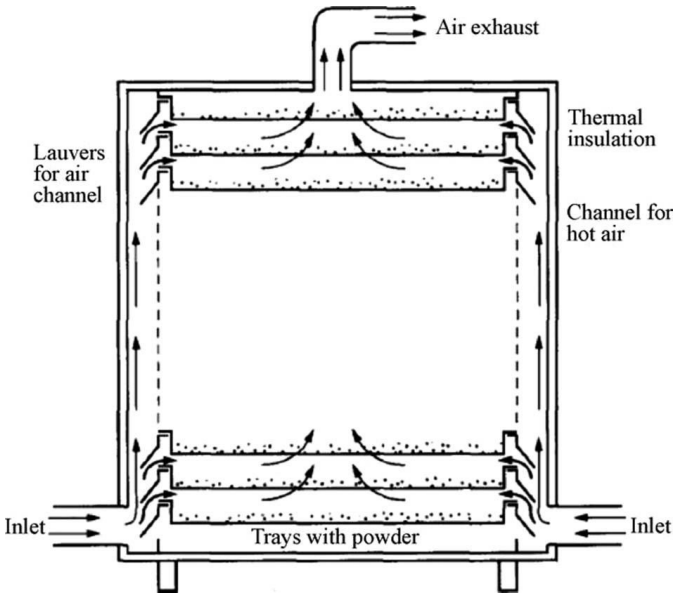

Fig 1.11: Mustard powder drying with forced flow air solar collector[11]

1.7.5 Tobacco drying

The tobacco drying system conventionally used wood chips as fuel thereby increasing carbon footprint. The solar drier use air as drying media and its potential has been demonstrated by many. The aluminum sheet corrugated to increase heat transfer to air has been designed. Double glass cover is used to reduce the moisture of the tobacco. Temperature range is of 55-77 degrees is kept. It was found that with solar drier there occurs 40% fuel savings and 25% drying time reduction.

[10]Mohanraj and Chandrasekar, Drying of copra in a forced convection solar drier, Biosystems Engineering, 99(4), pp. 604–607, 2008.
[11] Pawar et al., Solar drying of custard powder, Energy Conversion and Management, 36(11), pp. 1085–1096, 1995.

1.8 Moisture Control of crops

Moisture control is cardinal when it comes down to longer food preserve. Moisture controlled food could be stored for up to a whole year without facing complicated addling issues. Food storing capacity goes beyond a year or two.

Table 1.1: Allowed Moisture content in Food items.[12]

Crop	Initial Moisture	Final Moisture	Allowable Temperature(°C)
Maize	35	15	60
Wheat	20	16	45
Rice	24	11	50
Pulses	20-22	9-10	40-60
Oil seed	20-25	7-9	40-60
Green Peas	80	5	65
Cauliflower	80	6	65
Carrot	70	5	75
Corn	24	14	50
Apples	80	24	70

[12] □ □□r □□□□□□□d □□ □□ r □□□ □□r c □□□□□□ □□d c □□r d □□□□□□r r □□□□□□□□□ □□ *Int J Green Energy*, vol. 10, no. 7, pp. 690□738, 2013.

1.9 Challenges faced by Solar air heaters

Heat transfer to air increases overall efficacy of the heating process thereby reduction in conventional fuel consumption and less drying time. The advantageous have been demonstrated many times enthralling researchers to augment its latent potential. While the research is done extensively, there are various factors which impedes efficiency of solar air heater.

- Low Thermal conductivity of Air.
- Losses pertaining to glass and bottom plate of solar heater.
- Thermo-Hydraulic efficiency factor.
- Cloudy weather, Rainy day, Hazy day and blustered winds.
- Losses from inlet and outlet section.
- Shading effect from trees or nearby buildings.
- Inclination angle of irradiation keeps changing every day.
- Sleet and Hail as they scratch the glass cover thereby less radiation penetrates.

1.10 Thermal Properties of some common food

Table 1.2: Thermal properties of food.[13]

Food	Freezing Point	Sp.heat above freezing (kj/kg.k)	Sp.heat below freezing (kj/kg.k)	Latent heat of fusion (kj/kg.k)
Onions	-0.8	3.79	1.95	294
Peas	-0.6	3.32	1.77	247
Peeper	-0.7	3.92	2.00	307
Potato	-0.6	3.42	1.85	261
Apple	-1.1	3.65	1.90	281
Apricot	-1.1	3.69	1.91	284
Banana	-0.8	3.35	1.78	251
Grapes	-1.1	3.59	1.84	277
Lemons	-1.4	3.82	1.94	297
Olives	-1.1	3.35	1.78	251
Oranges	-0.8	3.75	1.94	291

The thermal properties rely heavily on moisture content of vegetables or fruits or spices. Various models have been studied by researchers to predict the moisture content in a vegetable at certain temperature of drying air.

[13] www.researchgate.net

1.11 Objectives of project undertaken

The ever increasing carbon footprint and the high alerts on energy regulation is a nightmare to [illegible] conventionally in drying market. The reduced cost and drying time are major factors attracting researchers to this field.

- To increase the thermal efficiency of solar flat plate collector by minimizing losses and controlling the Air flow rate entering the collector.

- Validating Model with Smooth rectangular Duct of solar collector and further continuing experimentation with artificial induced turbulence.

Chapter 2

Literature Review

2.1 Introduction

Solar air heaters latent potential is yet to be explored at industrial extent. Researchers are putting lot of resources in this area to reduce carbon footprint associated with conventional technology. This chapter gives reader insinuation about the work which is carried out on solar air heaters. This chapter deals with the previous work which is done on solar heaters and lays the very platform upon which the thesis is worked. The chapter puts light on the literature review of air heat transfer under various modifications of absorber plate, thermos-hydraulic efficiencies under various set-up combinations, Irradiation change influences solar heater efficiency and the inlet air properties effects air temperature inside the solar air heater.

Heat transfer to the air (working media) depends upon many factors which some are listed below:-

- Modifications on absorber plate.
- Different convection mode of air flow
- Black dull painting method on absorber plate.
- Air properties at inlet.
- Irradiation available.
- Inclination angle Respective to zone.
- Losses minimization pertaining to the glass cover and bottom plate.

Below is the literature studied corresponding to the parameters aforementioned above.

2.2 Modifications on absorber plate

The absorber plate is the zone where the incidented radiation is absorbed. The air coming in contact with the absorber plate gets heated up and rises up due to density difference. Temperature of the plate goes above 100°C at the peak radiation hours in a day (peak hours 12-3PM). Various methods have been adopted by researcher to increase the heat transfer from

absorber plate to air by modifying absorber plate surface with corrugation or by adding external media to the absorber plate to increase heat transfer to air for better efficiency.

Transverse wire rib roughness

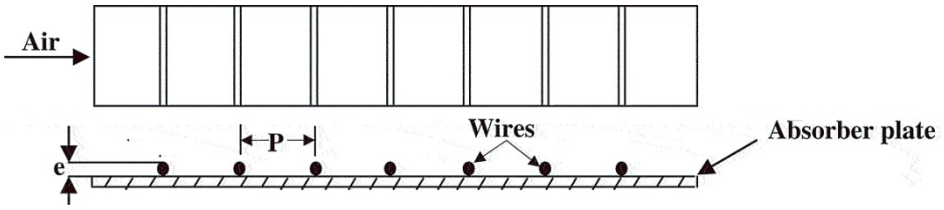

Fig 2.1: Wire rib Roughness [1].

Prasad and Mullick (1983) used protruding wires to enhance heat transfer rate to air.

- 14% improvement in thermal performance was reported over wide range of Reynold's Number.
- (P/e) range of 10–40 and relative roughness height (e/D) range of 0.01–0.03. Where P is Distance among wires and e is diameter of wires.

Wedge shaped rib roughness

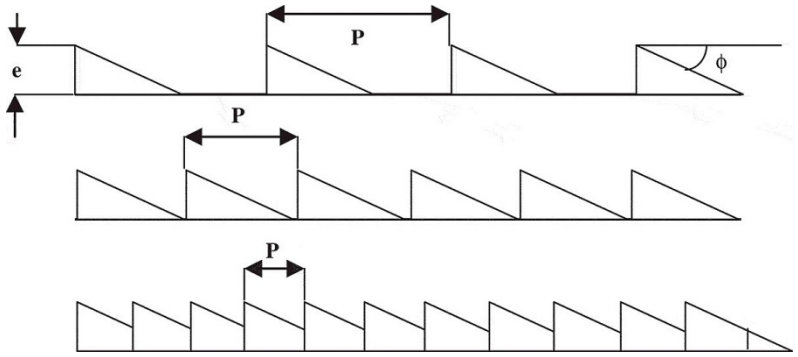

Fig 2.2: Wedge roughness on collector. [2]

Bhagoria, Saini, and Solanki (2002) did research on factors like friction, relative roughness influence on thermal heat transfer between absorber plate and air. Nusselt number up to 2.4 times while the friction factor rises up to 5.3 times of smooth Duct. Maximum Heat-

Transfer occurs at Relative roughness of 7.57. Maximum advancement is reached at wedge angle of 10 degree leading to maximum heat transfer rate.

Broken rib roughness

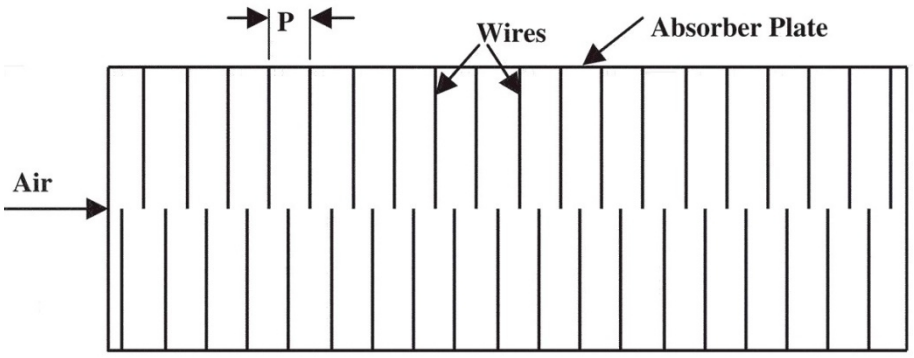

Fig 2.3: Broken rib roughness [3].

Sahu and Bhagoria (2005) performed experiments with thin wires installed on and over absorber surface. 1.25 - 1.5 times is the increase was observed in the Heat-Transfer coefficient at higher Reynold□s number compared to smooth rectangular duct. Depending upon flow conditions maximum thermal efficiency attainable is 51% at relative roughness of 0.038.

Inclined wire rib roughness

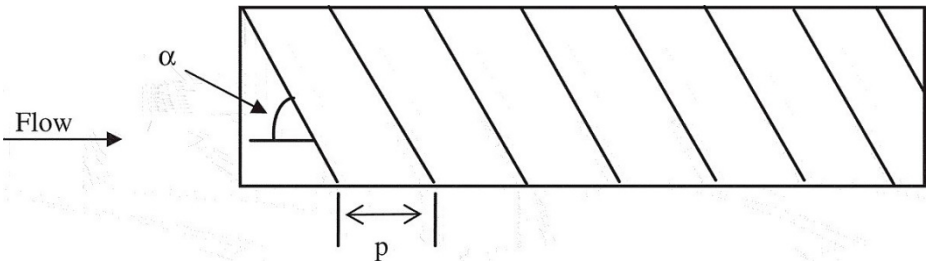

Fig 2.4: Inclined continuous rib roughness [4]

.

Gupta, Solanki, and Saini (1993) performed experiment to study the effects of modification on thermal performance of solar air heater. It was found that non-transverse type was having leverage over transverse rib roughness type solar heater. In comparison to simple rectangular duct heater the heat transfer was found 1.8 times and the friction 2.7 times higher when the ribs were placed at 60 and 70 degrees.

Inclined continuous ribs with gap

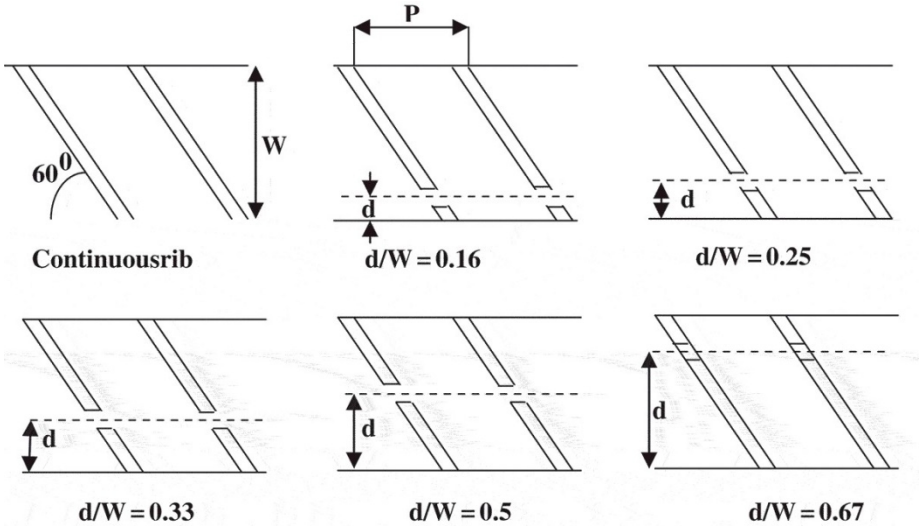

Fig 2.5: Inclined continuous rib roughness with gap [5].

Aharwal, Gandhi, and Saini (2009) experimented on this specific adjustment to comprehend the influence which this type of modification will have on heat transfer and friction factor of solar air heater. Maximum heat transfer occurs at relative gap position of 0.25 which accounts for 2.83 times the standard solar air heater. The very adjustment also increases the friction 3.86 times of standard solar air heater. Relative roughness was 0.0.37 and and angle of air induction 60 ⌈.

Transverse and incline rib roughness

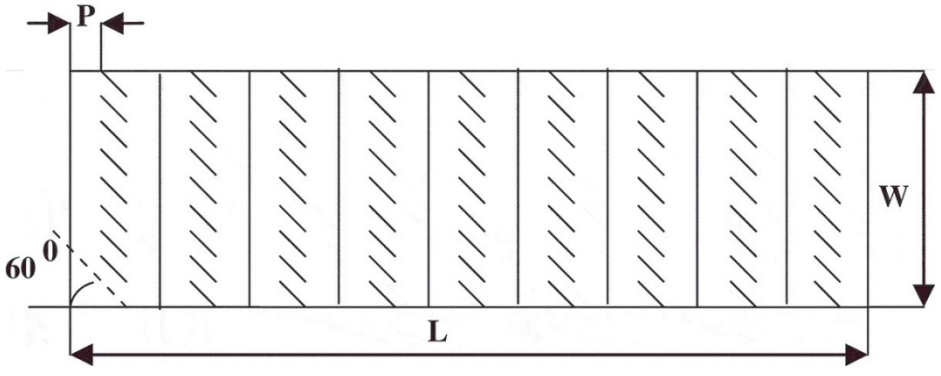

Fig 2.6: Combination of transverse and inclined rib roughness [6] [7].

Varun, Saini, and Singal (2008) did experiments with 3 different metals of ribs. Best results were observed at relative roughness pitch of 8 (p/e). Mittal and Varun (2009) extended the

research with same experimental set-up but with 3 different types of ribs geometry was used and it was concluded that optimal thermos-hydraulic efficiency occurs at relative roughness of 8.

Expanded metal mesh roughness

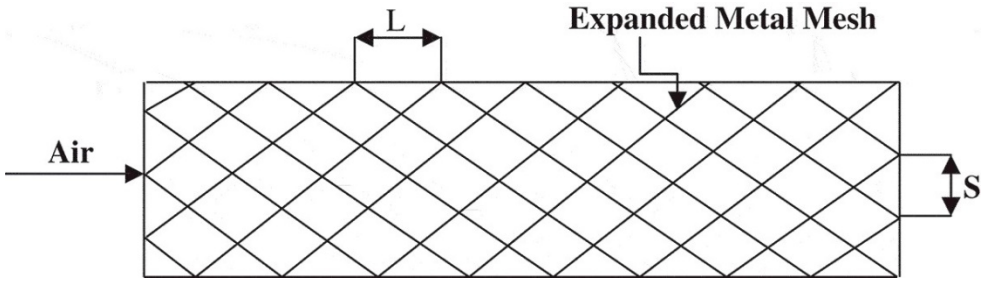

Fig 2.7: Expanded metal mesh roughness [8].

Saini and Saini (1997) performed experiments with fully turbulent flow in rectangular duct with mesh as turbulence inducer. Maximum heat transfer was obtained at 62 ⌈with relative long way mesh of 46.87 and short way mesh value of 25. Heat transfer value obtained is 300% compared to rectangular smooth duct air flow.

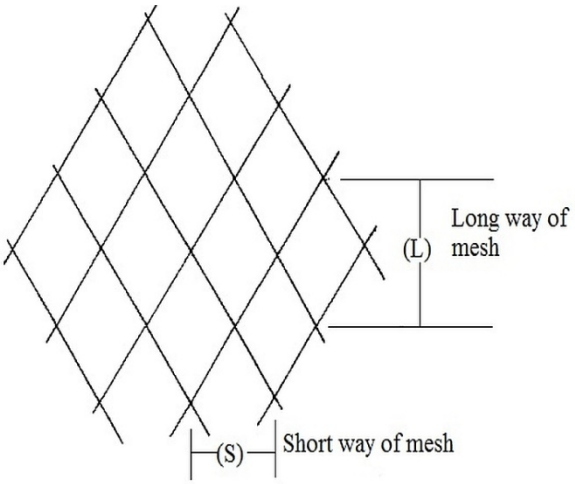

Fig 2.8: Geometry of expanded mesh [8].

Metal grit rib roughness

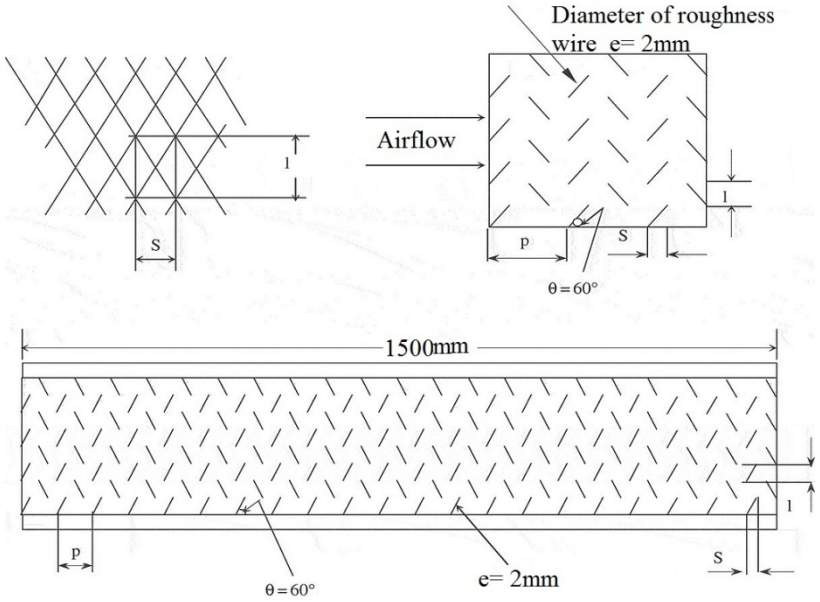

Fig 2.9: Metal grit rib roughness [9].

Karmare and Tikekar (2007) performed experiments with metal grit ribs in solar heater with aspect ratio of 10:1. The Nusselt number was found 2 times that of smooth rectangular duct. The parameters which yielded highest Nusselt number was e/D=0.044, Relative roughness=17.4, 1/s=1.73. Modifications also increased the friction factor by three fold. S= short way mesh value. P= Distance between two ribs. ¯ =60 ˉ angle of air entrance. e= wire diameter.

V-shaped rib roughness

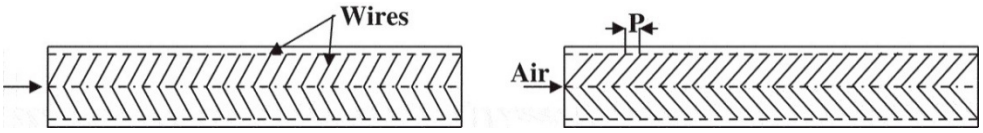

Fig 2.10: V-shaped Roughness [10].

Momin, Saini, and Solanki (2002) found experimentally that Nusselt number was 2.30 and roughness factor by 2.86 times at an angle of incidence of 60 ⌈. It was found that relative roughness of 0.034 and angle of attack 60 ⌈, V-shaped ribs improved Nusselt number by 1.14 and 2.30 times over inclined ribs and smooth plate at Reynolds number of 17034.

Staggered discrete V-shaped rib roughness

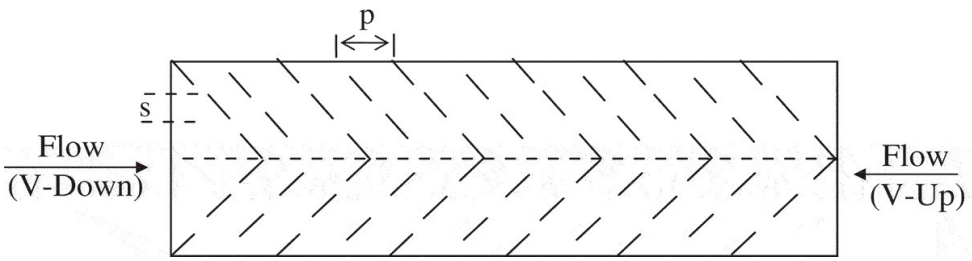

Fig 2.11: Staggered discrete V-shaped rib roughness [11].

Muluwork (2000) concluded that V-down flow gives better Nusselt number than V-up flow. Relative roughness of staggered V-ribs when increased the Nusselt number also increased and is maximum at relative roughness of 0.6. Maximum heat transfer occurred at air incidence of 60 ⌈. Friction attained apex value at angle of attack of 70 ⌈.

Multi V-shaped rib roughness

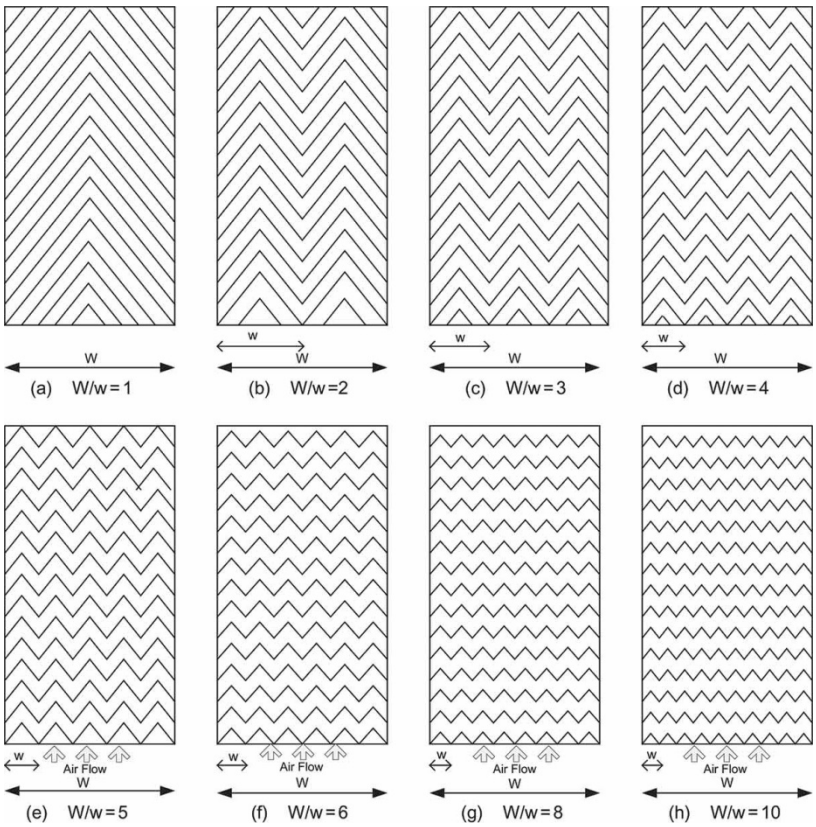

Fig 2.12: Multi V-shaped roughness [12].

Hans, Saini, and Saini (2010) studied three parameters namely; relative roughness width (W/w), relative roughness pitch (P/e), relative roughness height (e/D) and found that maximum heat transfer occurs for relative roughness width value 6 while friction factor maximum value for relative roughness width value 10. It was found Nusselt number and friction factor c rr d c . Maximum increase of Nusselt number and friction factor observed at relative roughness pitch (P/e) of 8 while Nusselt number and friction factor increase with the value of relative roughness height (e/D).

Multi V-shaped rib roughness with gap

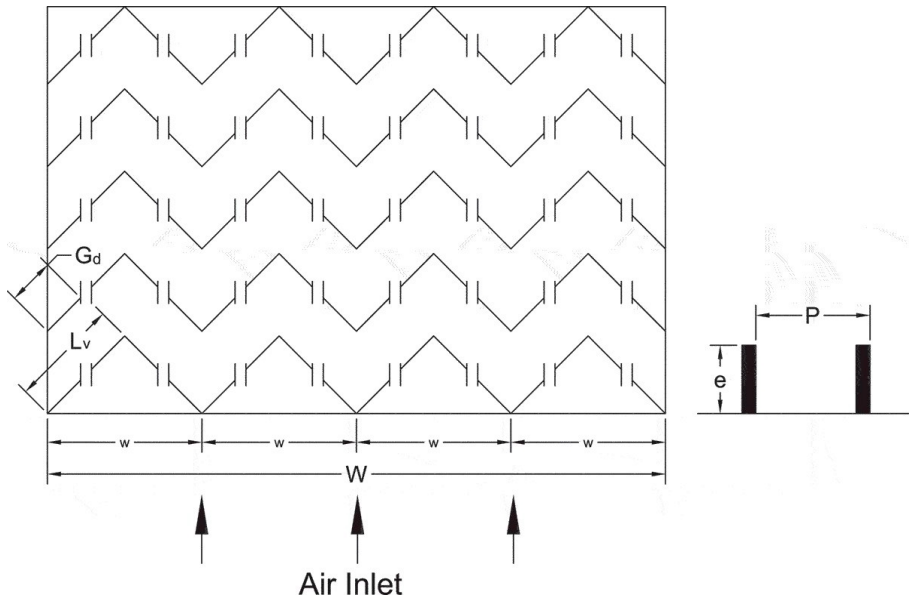

Fig 2.13: Multi V-shaped rib roughness with gap [13].

Kumar, Saini, and Saini (2012) conducted experiments and compared the results with performance of solar air heater with V-shape rib and Multi V-shape rib. Nusselt number and friction factor were 6.32 and 6.12 times that of smooth duct. The thermo-hydraulic efficiency parameter was best for the relative gap distance of 0.69 and the relative gap width of 1.0. The apex friction factor value occurred for multi v-shaped with gap rib at relative roughness width value 10.

Arc shaped rib roughness

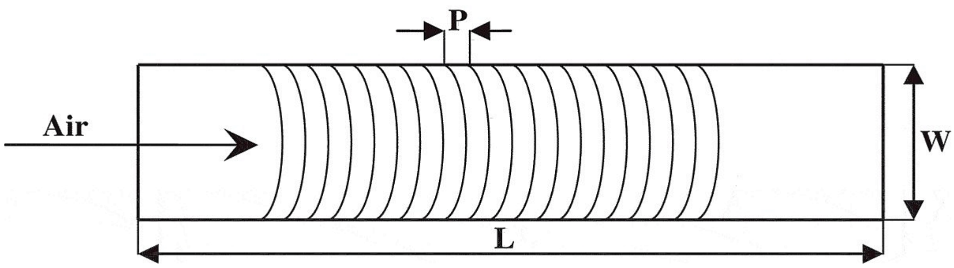

Fig 2.14: Arc shaped roughness [14].

Saini and Saini (2008) concluded the maximum advantage in Nusselt number achieved 3.80 times pertaining to □rc□□□□□□□□□□□□□□□□□□□□□□□□□□□□□□ at relative roughness height of 0.0422. Although, the friction factor germane to these parameters was observed 1.75 times only leading to less pumping power consumption.

Dimple shaped rib roughness

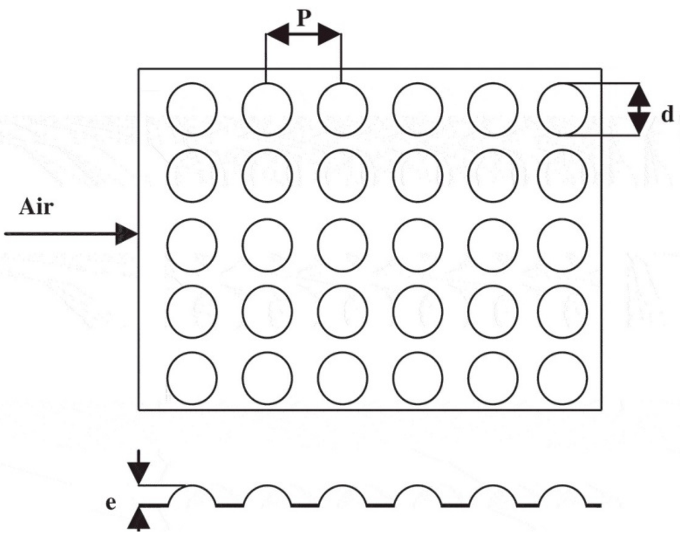

Fig 2.15: Dimple-shaped rib roughness [15].

Saini and Verma (2008) performed experiments on the dimple shaped turbulence inducer solar air heater. Nusselt number hit zenith value corresponding to relative roughness height (e/D) of 0.0379 and relative roughness pitch (P/e) of 10. While friction factor sit at nadir

position corresponding relative roughness height (e/D) of 0.0289 and relative roughness pitch (P/e) 10. e = Roughness height.

Rib-grooved roughness

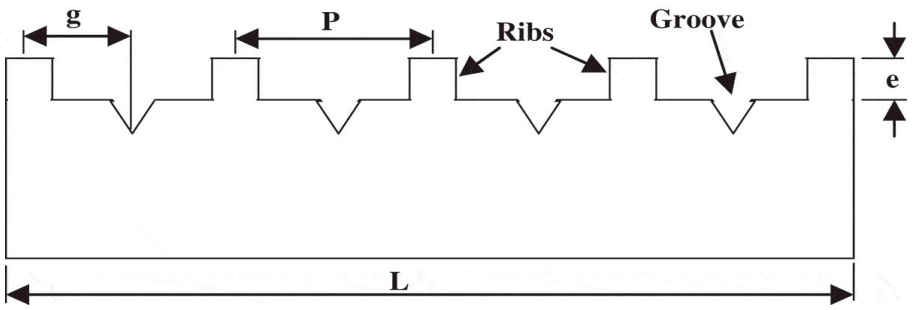

Fig 2.16: Rib-grooved artificial roughness [16].

Jaurker, Saini, and Gandhi (2006) performed experiments on broad wall. It was found that Nusselt number and friction factor were 2.7 and 3.6 times respectively comparison to smooth absorber plate. Maximum heat transfer was for relative roughness pitch (P/e) 6 and relative groove (g/P) of 0.4. The artificial roughness of this specific type yielded best thermos-hydraulic performance of solar air heater studied.

Chamfered rib-grooved roughness

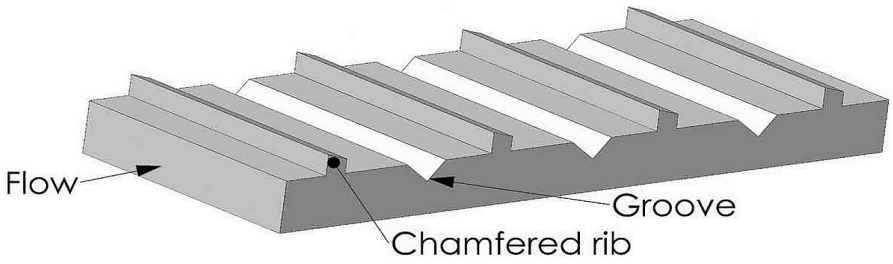

Fig 2.17: Chamfered rib-grooved roughness [17].

Layek, Saini, and Solanki (2007) performed modifications on solar air heater with chamfered ribs. It was concluded that Nusselt number and friction factor increased 3.24 and 3.78 times respectively compared to smooth duct. Heat transfer maximized at relative roughness

pitch of 6 and relative groove position of 0.4. Highest Nusselt number occurred at chamfer angle of 18^{o} but the friction factor increase linearly with increase in chamfer angle.

W-shaped rib roughness

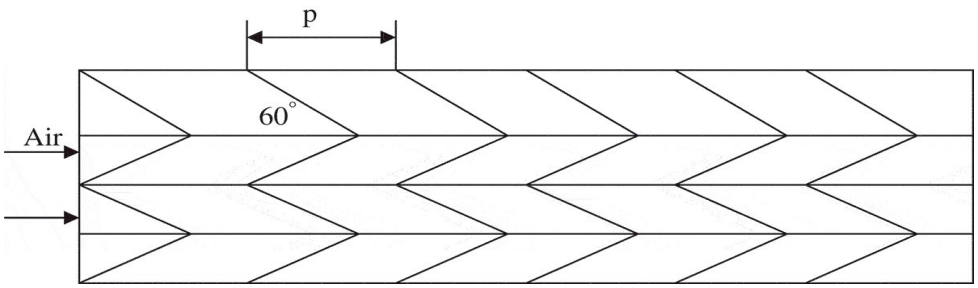

Fig 2.18: W-shaped rib roughness [18].

Lanjewar, Bhagoria, and Sarviya (2011) investigated rectangular duct W-shaped rib roughened solar air heater. W-shaped ribs were tested in downstream W-down and W- up to the flow. Maximum Nusselt number was 2.36 for angle of attack of 60 ⌈ for W-down ribs and 2.24 for angle of attack of 60 ⌈ for W-up flow compared to smooth plate. P is the distance between adjacent W-shaped ribs. ¯ is the angle of attack. Maximum thermo-hydraulic performance W-down ribs 1.98 and was 1.81 for W-up ribs.

Discrete W-shaped rib roughness

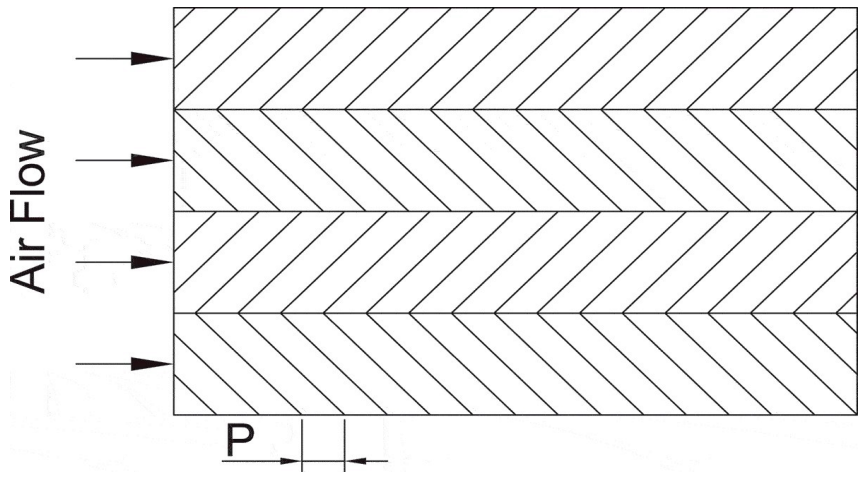

Fig 2.19: Discrete W-shaped rib roughness [19].

Kumar, Bhagoria, and Sarviya (2009) conducted experiments on one wall of absorber plate with discrete W-shaped ribs. The solar air heater with aspect ratio of 8:1 (Aspect ratio = width/height). Nusselt number and friction factor as a result of artificial roughness was found to be 2.16 and 2.75 times that of smooth duct for an attack angle of 60^{o} and relative roughness height of 0.0338.

Transverse continuous/broken and V-shaped broken rib roughness

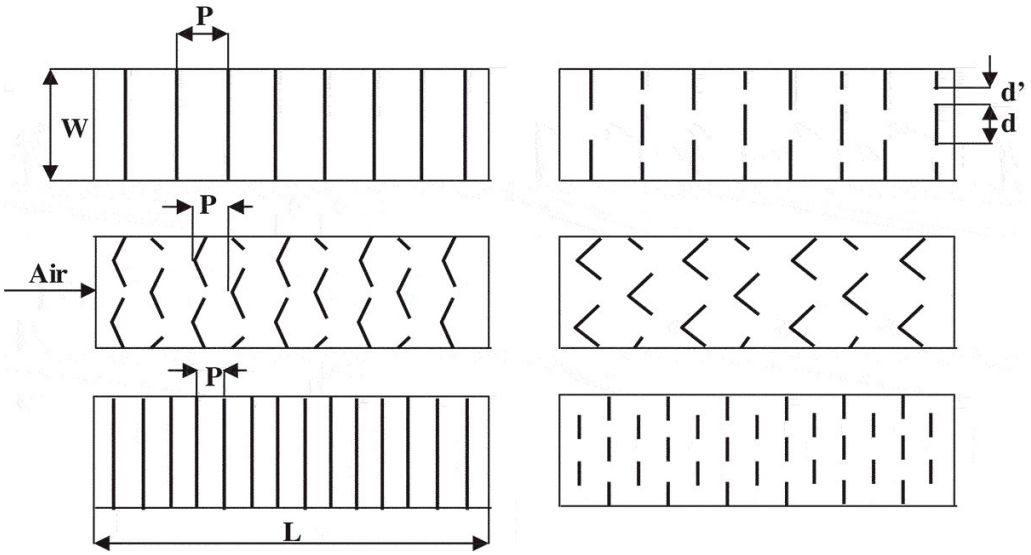

Fig 2.20: Transverse continuous/broken and V-shaped broken roughness [20].

Tanda (2011) performed experiment with one wall of absorber section dresses with ribs while other three walls were kept smooth. All configurations performed better than smooth channel in medium-low range of the Reynolds number. Roughening the heat transfer surface by transverse broken ribs was concluded apposite het transfer enhancement technique of the investigated rib geometries. P is pitch; Distance between two adjacent ribs.

2.3 Different Convection Modes

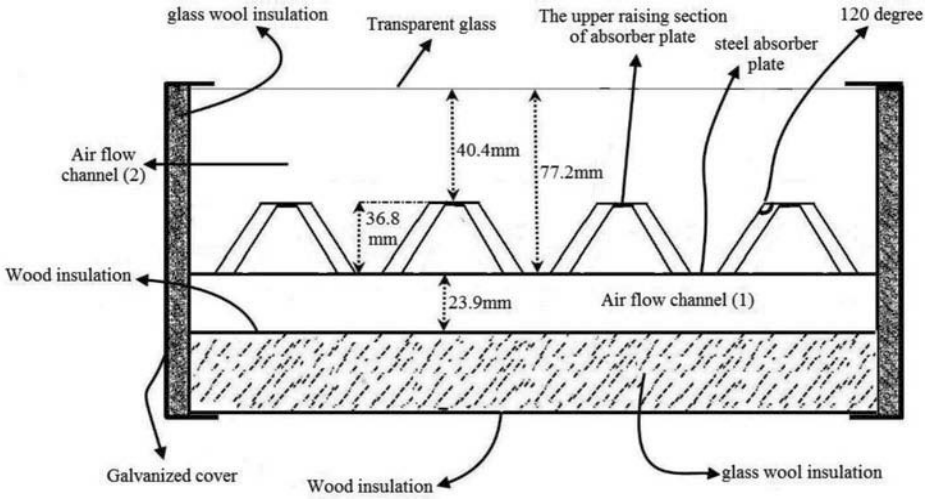

Fig 2.21: Schematic cross section of air solar collector [21].

Amir Hematian & Amir Abbas Bakhtiari (2015) maximum collector ef□c□□□c□ occurred at the time of 12-2 in natural convection. This can be explained by the maximum air temperature difference between the inlet and outlet of collector and also the higher rate of mass □□□ due to density difference. Irradiation is maximum during this time of the day.

The average ef□c□□c□□□□solar air collector has an ascending tendency, and only at peculiar intervals, i.e. at time 12:00□13:00, 14:00□15:00, and 19:00□20:00 at local time there are descending streaks in it. The streaks are due to sudden changes in weather conditions and which affects average inlet and outlet air temperatures.

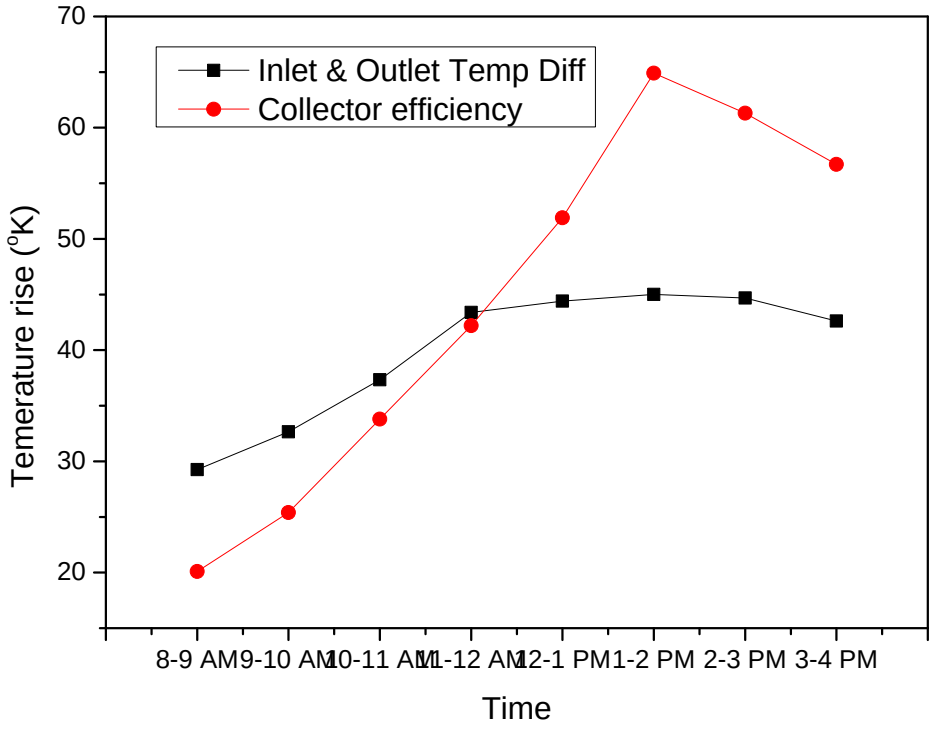

Fig 2.22: Collector efficiency and Temperature rise graph in natural convection mode [21].

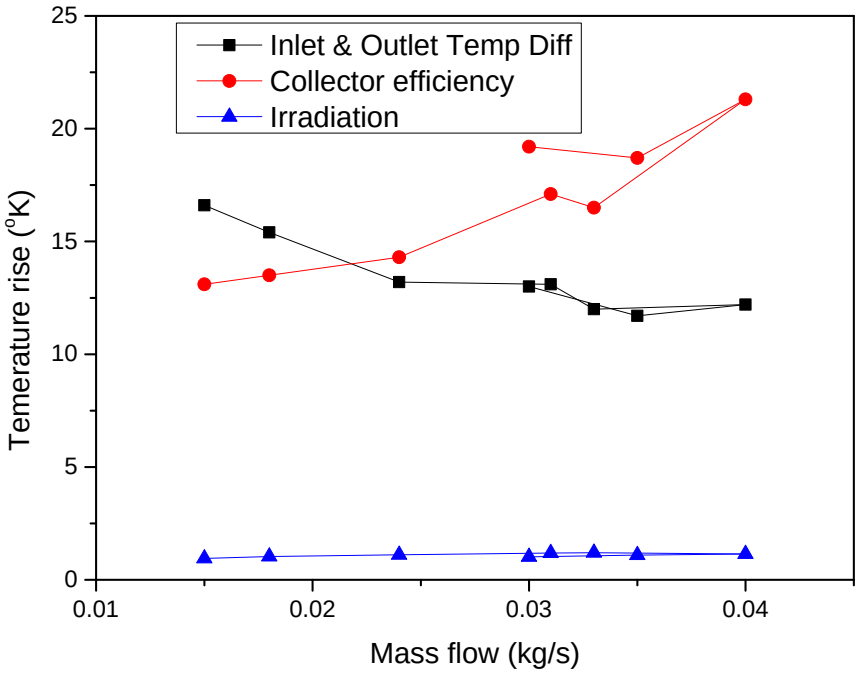

Fig 2.23: Collector efficiency & Temperature rise corresponding to mass flow rate in forced convection mode [21].

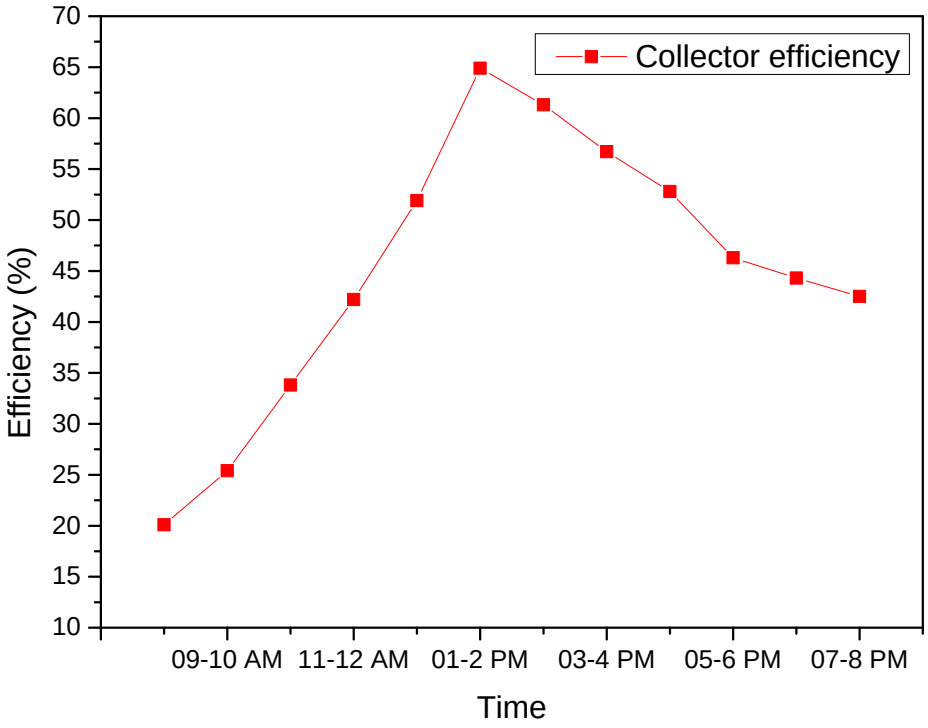

Fig 2.24: Collector efficiency during natural convection mode [21].

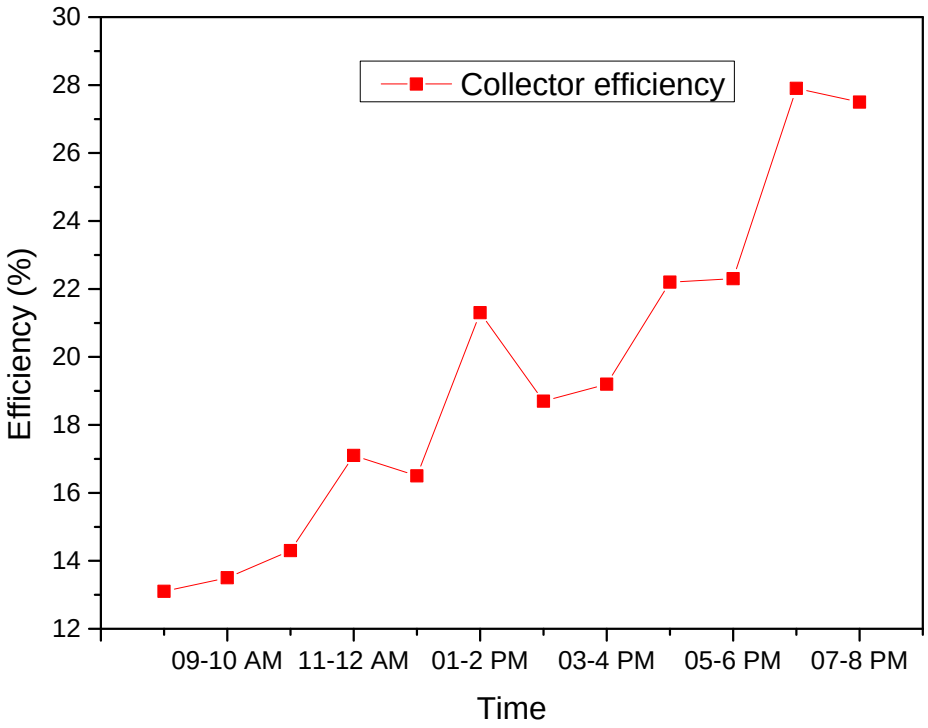

Fig 2.25: Collector efficiency variation in forced convection mode [21].

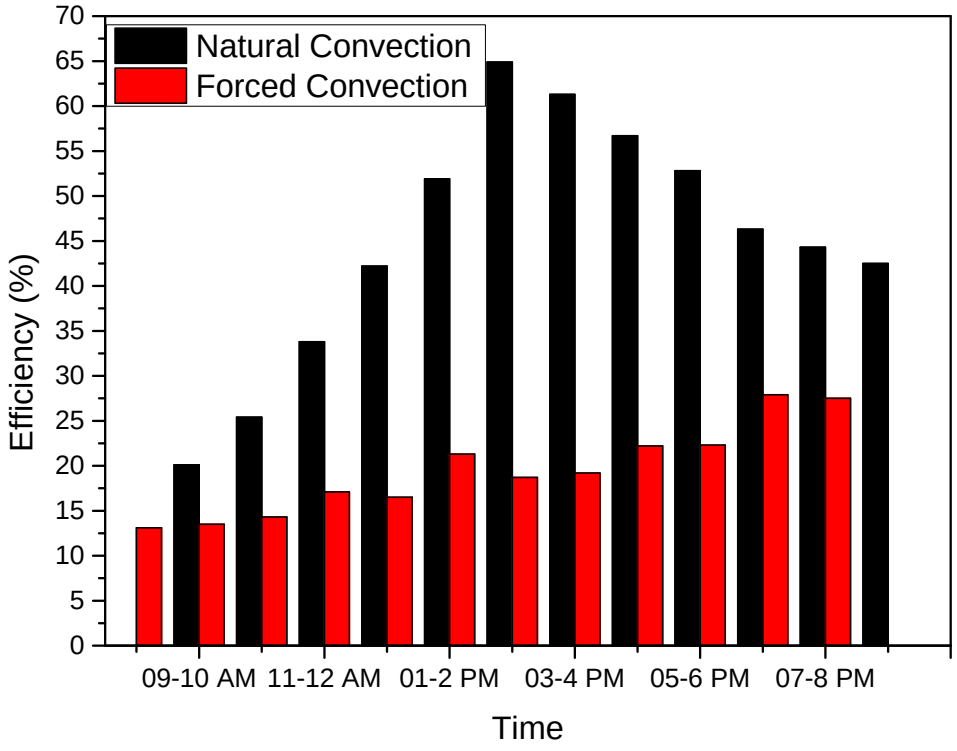

Fig 2.26: Efficiency comparison in natural and forced convection of air [21].

2.4 Coating of absorbing material on absorber plate

Materials mainly used are copper, Stainless steel (304 grade), Aluminum, Iron for making the absorber part of solar air heater. The coating of dull black color paint on the absorber plate is very decisive factor in the performance of solar air heater. More and more sophisticated methods have been developed hunching absorbing capacity of absorbing plate over 95-98%.

J.Vuletin (1989) first shed light on this factor taking copper as absorbing material. Copper oxide coatings were made using chemical and electro-chemical processes. The black surface is made by direct chemical reaction of chemical copper substrate with absorber section. Copper substrate is immersed in salt solution of sodium hydroxide (NaOH) at temperature of 70-80 $^{\circ}$C for about 1 minute. Three samples of coating material on copper plate were made by changing immersing time of the copper substrate in salt solution of sodium hydroxide.

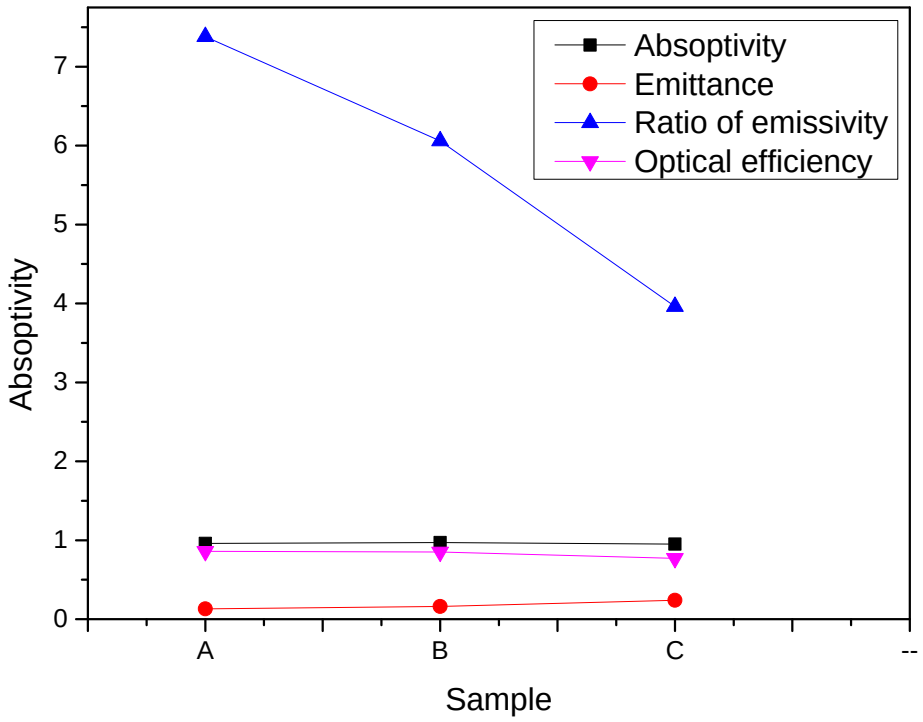

Fig 2.27: Comparison of three samples on absorptivity, emittance, ratio of emissivity and optical efficiency [22].

.

2.5 Hybrid Solar air heater to minimize losses

Reflector is used to curb losses related to glass cover. Since double glass cover has air inside it which conducts heat thereby increasing glass cover temperature and glass cover start losing heat by radiation to atmosphere. With reflector the incidented radiation increases on solar absorbing plate leading to higher temperature and increased heat transfer from absorber to air. Reflector reflects the leaving radiation back to the solar air heater thereby reducing losses.

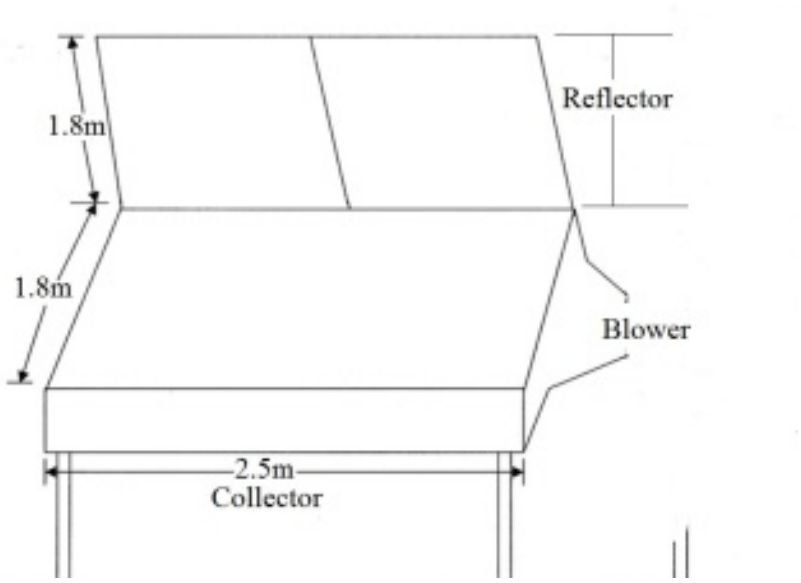

Fig 2.28: Hybrid solar air heater [23].

Different convection modes were tested to analyze the performance behavior of solar air heater. Convection modes details as follows:

Mode 1 = Daytime using solar radiation but night time drying ambient air.

Mode 2 = Daytime solar drying and storing heat in storage tank and recirculating hot water from the storage tank in the night.

Mode 3 = Daytime solar drying and storing heat in storage tank recirculating hot water from the storage tank and using external water heating in night.

Mode 4 = In inclement weather, day and night time drying hot water in the collector using water heater.

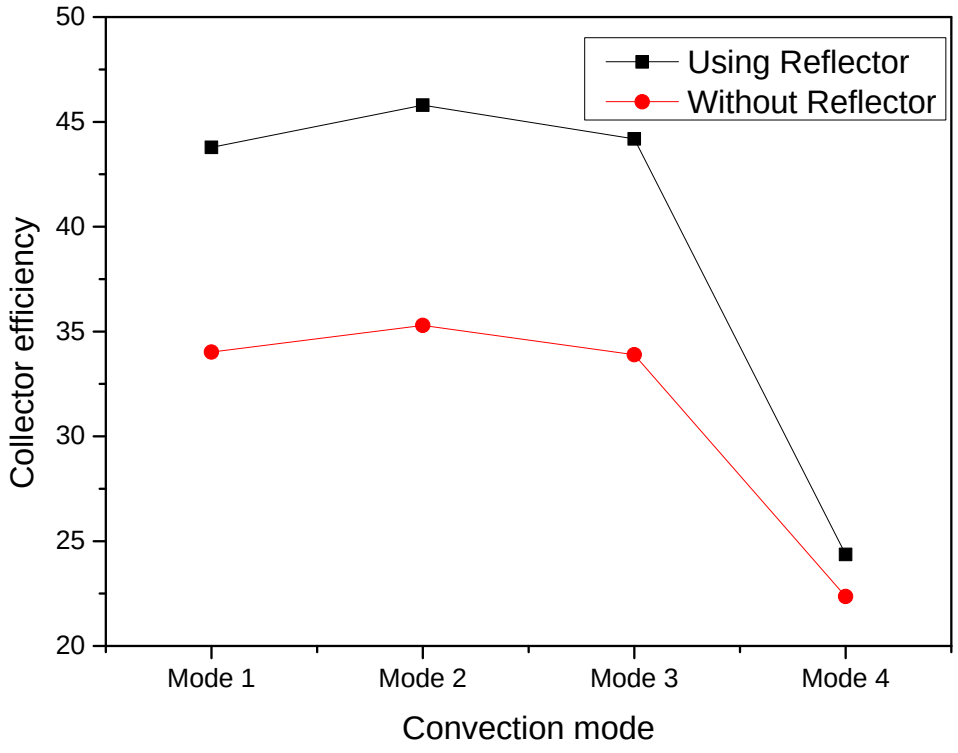

Fig 2.29: Comparison of collector efficiency at different convection modes [23].

References

1. Prasad K., and S.C. Mullick. 1983. Heat transfer characteristics of a solar air heater used for drying purposes. *Applied Energy* 13 (2): 83-93.
2. Bhagoria, J.L., J.S. Saini, and S.C. Solanki. 2002. Heat transfer coefficient and friction factor correlations for rectangular solar air heater duct having transverse wedge shaped rib roughness on the absorber plate. *Renewable Energy* 25 (3): 341-369.
3. Sahu, M.M., and J.L. Bhagoria. 2005. Augmentation of heat transfer coefficient by using 90^{o} broken transverse ribs on absorber plate of solar air heater. *Renewable Energy* 30 (13): 2057-2073.
4. Gupta, D., S.C. Solanki, and J.S. Saini. 1993. Heat and fluid flow in rectangular solar air heater ducts having transverse rib roughness on absorber plates. *Solar Energy* 51 (1): 31-37.
5. Aharwal, K.R., B.K. Gandhi, and J.S. Saini. 2009. Heat transfer and friction characteristics of solar air heater ducts having integral inclined discrete ribs on absorber plate. *International Journal of Heat and Mass Transfer* 52 (25-26): 5970-5977.
6. Varun, R.P. Saini, and S.K. Singal. 2008. Investigation of thermal performance of solar air heater having roughness elements as a combination of inclined and transverse ribs on absorber plate. *Renewable Energy* 33 (6): 1398-1405.
7. Mittal, M.K., and Varun. 2009. Thermohydraulic performance of solar air heater provided with artificial roughness on the absorber plate. *Institute of Engineers Journal IE (I)–MC* 92 (July): 43-48.
8. Saini, R.P. and Saini, J.S. Heat transfer and friction factor correlations for artificially roughened ducts with expanded metal mesh as roughness element. *International Journal of Heat and Mass Transfer 40*, 4 (1997), 973–986.
9. Karmare, S.V., and A.N. Tikekar. 2007. Heat transfer and friction factor correlation for artificially roughened duct with metal grit ribs. *International Journal of Heat and Mass Transfer* 50 (21-22): 4342–4351.
10. Karwa, R., S.C. Solanki, and J.S. Saini. 1999. Heat transfer coefficient and friction factor correlations for the transitional flow regime in rib-roughened rectangular ducts. *International Journal of Heat and Mass Transfer* 42 (9): 1597-1615.

11. Momin, A.M.E., J.S. Saini, and S.C. Solanki. 2002. Heat Transfer and Friction in Solar Air Heater Duct with V-Shaped Rib Roughness on Absorber Plate. *International Journal of Heat and Mass Transfer* 45 (16): 3383-3396.
12. Muluwork, K.B. 2000. Investigations on fluid flow and heat transfer in roughened absorber solar heaters. PhD dissertation, IIT Roorkee, India.
13. Hans, V.S., R.P. Saini, and J.S. Saini. 2010. Heat transfer and friction factor correlations for a solar air heater duct roughened artificially with multiple v-ribs. *Solar Energy* 84 (6): 898-991.
14. Singh, S., S. Chander, and J.S. Saini. 2011. Heat transfer and friction factor correlations of solar air heater ducts artificially roughened with discrete v-down ribs. *Energy* 36 (8): 5053-5064.
15. Kumar, A., R.P. Saini, and J.S. Saini. 2012b. Experimental investigation on heat transfer and fluid flow characteristics of air flow in a rectangular duct with multi v-shaped rib with gap roughness on the heated plate. *Solar Energy* 86 (6): 1733-1749.
16. Saini, S.K., and R.P. Saini. 2008. Development of correlations for nusselt number and friction factor for solar air heater with roughened duct having arc-shaped wire as artificial roughness. *Solar Energy* 82 (12): 1118-1130.
17. Saini, R.P., and J. Verma. 2008. Heat transfer and friction factor correlations for a duct having dimple-shaped artificial roughness for solar air heaters. *Energy* 33 (8): 1277-1287.
18. Jaurker, A.R., J.S. Saini, and B.K. Gandhi. 2006. Heat transfer and friction characteristics of rectangular solar air heater duct using rib-grooved artificial roughness. *Solar Energy* 80 (8): 895-907.
19. Layek, A., J.S. Saini, and S.C. Solanki. 2007b. Heat transfer and friction characteristics for artificially roughened ducts with compound turbulators. *International Journal of Heat and Mass Transfer* 50 (23-24): 4845□4854.
20. Lanjewar, A., J.L. Bhagoria, and R.M. Sarviya. 2011a. Experimental study of augmented heat transfer and friction in solar air heater with different orientations of w-rib roughness. *Experimental Thermal and Fluid Science* 35 (6): 986-995.
21. Kumar, A., J.L. Bhagoria, and R.M. Sarviya. 2009. Heat transfer and friction correlations for artificially roughened solar air heater duct with discrete w-shaped ribs. *Energy Conversion and Management* 50 (8): 2106□2117.

22. Tanda, G. 2011. Performance of solar air heater ducts with different types of ribs on the absorber plate. *Energy* 36 (11): 6651-6660.

23. Hematian, A. and Bakhtiari, A. Efficiency Analysis of an Air Solar Flat Plate Collector in Different Convection Modes. *International Journal of Green Energy 12,* 9 (2015), 881–887.

24. Vuletin, J. et al. 1989. Chemical and optical properties of a black copper absorber for flat plate collectors. *Solar Energy Materials*. 19, 3-5 (1989), 249–256.

25. Hossain, M., Amer, B., and Gottschalk, K. Hybrid Solar Dryer for Quality Dried Tomato. *Drying Technology 26,* 12 (2008), 1591–1601.

Chapter 3

Computational Fluid Dynamics (CFD) Modeling

3.1 Introduction

Computational fluid dynamics is simulating software to predict the behavior of fluids, Structures, Stress variations and many more under the forces applied. This chapter gives an insight to the reader the various parameters that have been used to predict the temperature, Velocity and other parameters profile under the stipulated conditions. The CFD is used to analyze the air (working fluid) behavior under the natural and forced convection flow of air inside the solar air heater. Plots have been presented depicting the temperature profiles of air inside the device. Model is also validated comparing the results with data from other r□□□rc□r□□□r□□ CFD modeling results are compared with experimental results of researchers working on solar air heater in Iran. Based upon the CFD modeling fabrication of the model is also done which is presented in the next chapter. Hematian, A. and Bakhtiari, A. (2015) research is used to compare the results.

CFD modal is applied on the geometry created in Creo with different parameters to obtain the desired results. The chapter also gives insight to the different models used to predict the flow of the air inside the solar air heater.

3.2 Model Preparation

CFD model comprises of various steps assembled together and then applied on the boundary conditions to simulate the behavior of air. The following steps were taken to make a model in CFD model:-

- Geometry preparation.
- Meshing of Geometry model under analysis of fluent.
- Models to predict flow behavior.
- Materials defining of components.
- Cell zone conditions
- Boundary conditions
- Results.

3.2.1 Geometry preparation

The geometry of the solar air heater comprises of these parts:-

- Inlet cover.
- Outlet cover.
- Absorber plate.
- Bottom plate.
- Glass cover.
- Insulation.
- Glazed sheets.

Inlet cover

The inlet cover is the part from which air enters the set-up. Usually the temperature of air is simpatico with ambient temperature unless heated externally before entry. The cover is sometimes artificially roughened to enhance the turbulence right from the very starting of □r′ Ⅰemba·king jou·ney.

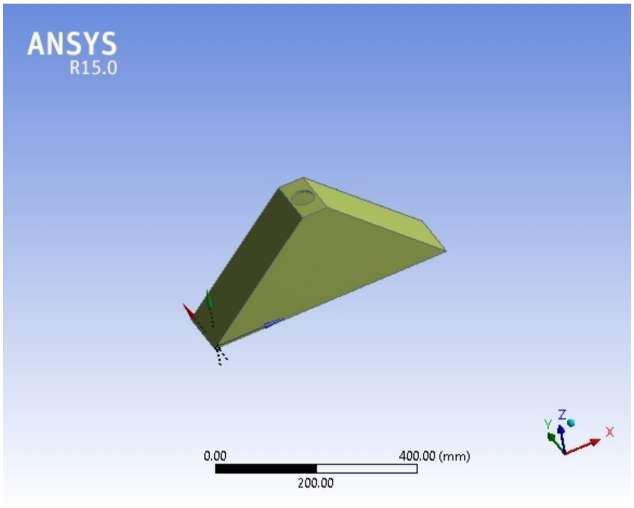

Fig 3.1: Inlet cover of solar air heater.

Outlet cover

The outlet cover is the part of solar air heater from where the heated air leaves the set-up. It is insulated in some cases to reduce the radiation losses from the walls of outlet cover. It is made of glazed iron sheet. Roughening in the outlet section leads to increased heat losses hence it is kept smooth while making the CFD model.

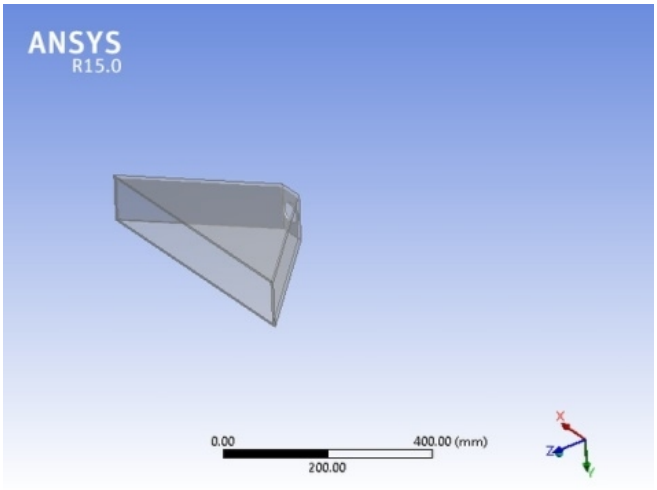

Fig 3.2: Outlet cover of solar air heater.

Absorber plate

The absorber plate is the heart of the solar air heater. It gets heated up r□□□□r□□□□□ to the air. The better the conductivity of the plate more heat flows to air. Mainly it is made of copper, aluminum, or stainless steel.

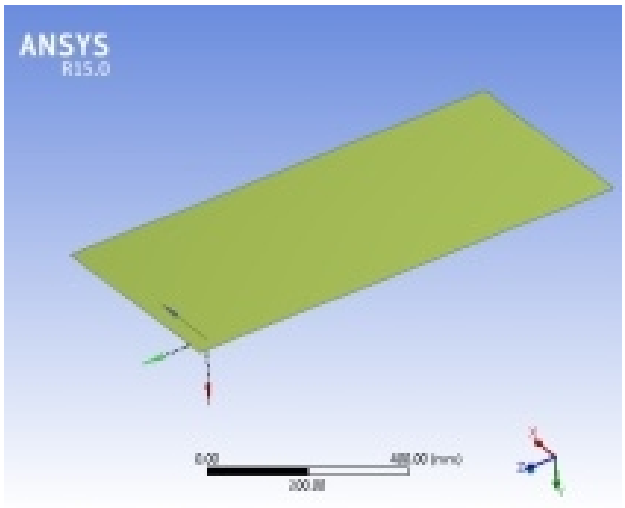

Fig 3.3: Absorber plate of steel of solar heater.

Bottom plate

Bottom plate is made of glazed iron sheet. Convection occurs on this section of the plate. Conduction losses are minimized with expanded polystyrene sheet. Insulation is filled all over the plate.

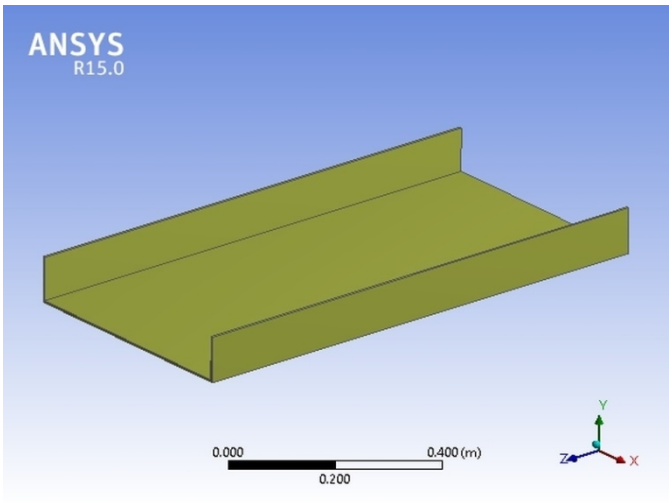

Fig 3.4: Bottom sheet of the solar air heater.

Glass cover

Glass cover on top reduces the losses by radiation by not allowing long wavelength radiation through the mirror. Toughened or simple mirror could be used for the purpose. Mirror with transmissivity of 98% is used. Two glass covers are used to curb the conduction losses as well.

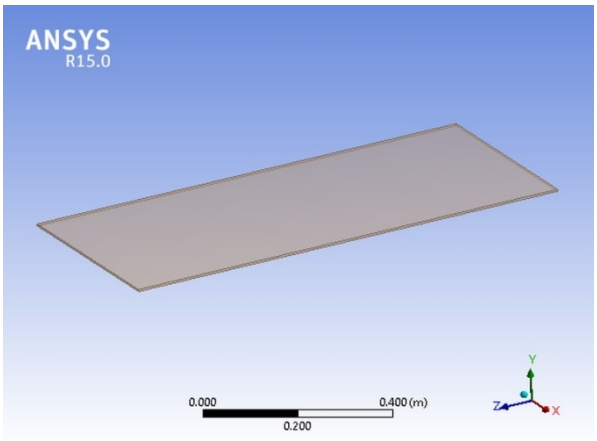

Fig 3.5: Glass cover at top of solar air heater.

Solar air heater model

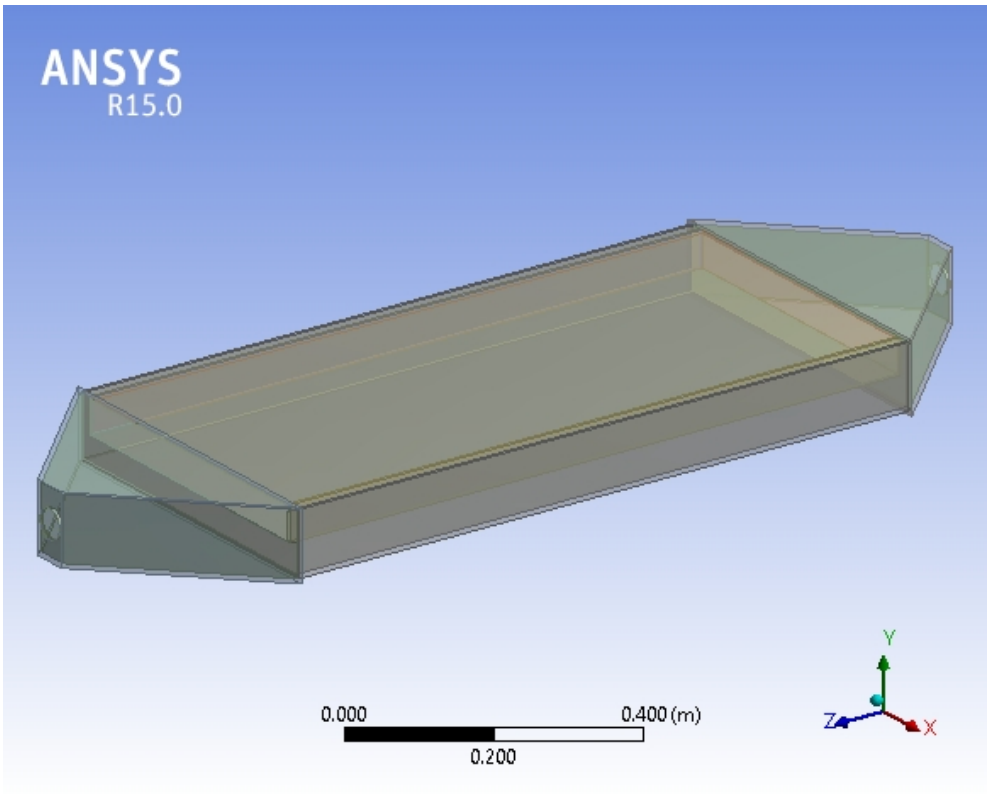

Fig 3.6: Model of solar air heater.

The model comprises of parts mentioned earlier. Air enters the inlet cover and flows over absorber plate with black colored dull paint deposited over it. Absorber plate delivers heat to the air. The behavior of air is predicted with various fluid prediction modals. Heated air leaves the set-up from outlet cover which could be used for various other purposes.

Dimensions of the geometry

Table 3:1: Dimensions of Solar model.

Part	Length (mm)	Breadth (mm)	Height (mm)	Thickness (mm)
Glazed Sheet	1000	500	100	5
Insulation	1000	490	95	15 & 50
Absorber plate	1000	450	0.5	0.5
Iron Sheet	1000	5	45	5
Glass Cover	1000	450	5	5
Inlet/Outlet cover	250	510	110	5

3.2.2 Meshing of the model

Meshing of the model is done with tetrahedron elements for better efficiency meshing. The elements of meshing 646860 and nodes of elements are 116908. Meshing is done with soft behavior under sizing of mesh. Relevance center is set to fine under sizing so as to have higher optimal prediction chances. Element size is under sizing is tested with two variations; 5 & 10 mm.

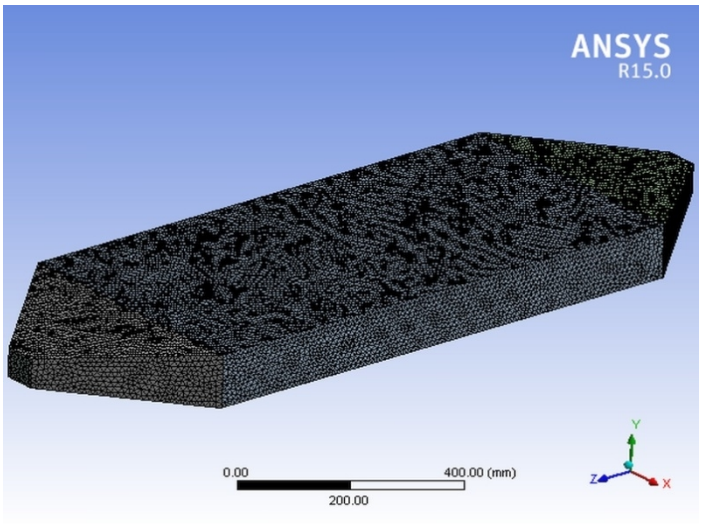

Fig 3.7: Meshing of model.

Boundary Conditions used in CFD modeling

Table 3.2: Boundary conditions used in modeling.

Absorber Section	Shear condition No slip	DTSR Model on	Wall thickness 0.1 mm	Momentous heating	
Inlet Air	Velocity= cm/s cm/s	Turbulent intensity 10%	Turbulent viscosity ratio 10	Inlet temperature 27°	Velocity specification magnitude normal to boundary
Outlet Air	Type pressure outlet	Backflow Turbulent intensity 10%	Backflow Turbulent viscosity ration 10	Backflow temperature 27°	Backflow magnitude normal to boundary
Outlet Section of Solar Air collector	Convection 40w/m^2	Free stream temperature	Stationary wall		
Inlet section of Solar air Collector	Convection 40w/m^2	Free stream temperature	Stationary wall	Inlet cover Galvanized iron	outlet cover Galvanized iron
Absorber	Radiation model	Solar Ray Tracing	Velocity (cm/s)	Absorber Material	
	DTSR	33° N 53° E G.M.T +3.30	c c	Steel copper	

- The DTSR radiation model is chosen because it takes into account the black body absorbing behavior of absorber plate.
- Convection rate is taken from air properties chart blowing at 5-10m/s.
- K-ἐ 2-Eqn was used in all the simulations and it gave reasonable results under the simulated conditions.
- d r r to wide range of fluids therefore aforementioned model was used in all further simulations.
- K- ἐ model predicted the temperature variations in the air flow inside solar flat Plate collector with amenable deviations from the experimental results.

3.2.3 Results of modeling

The results obtained from simulating the flow as follows:-

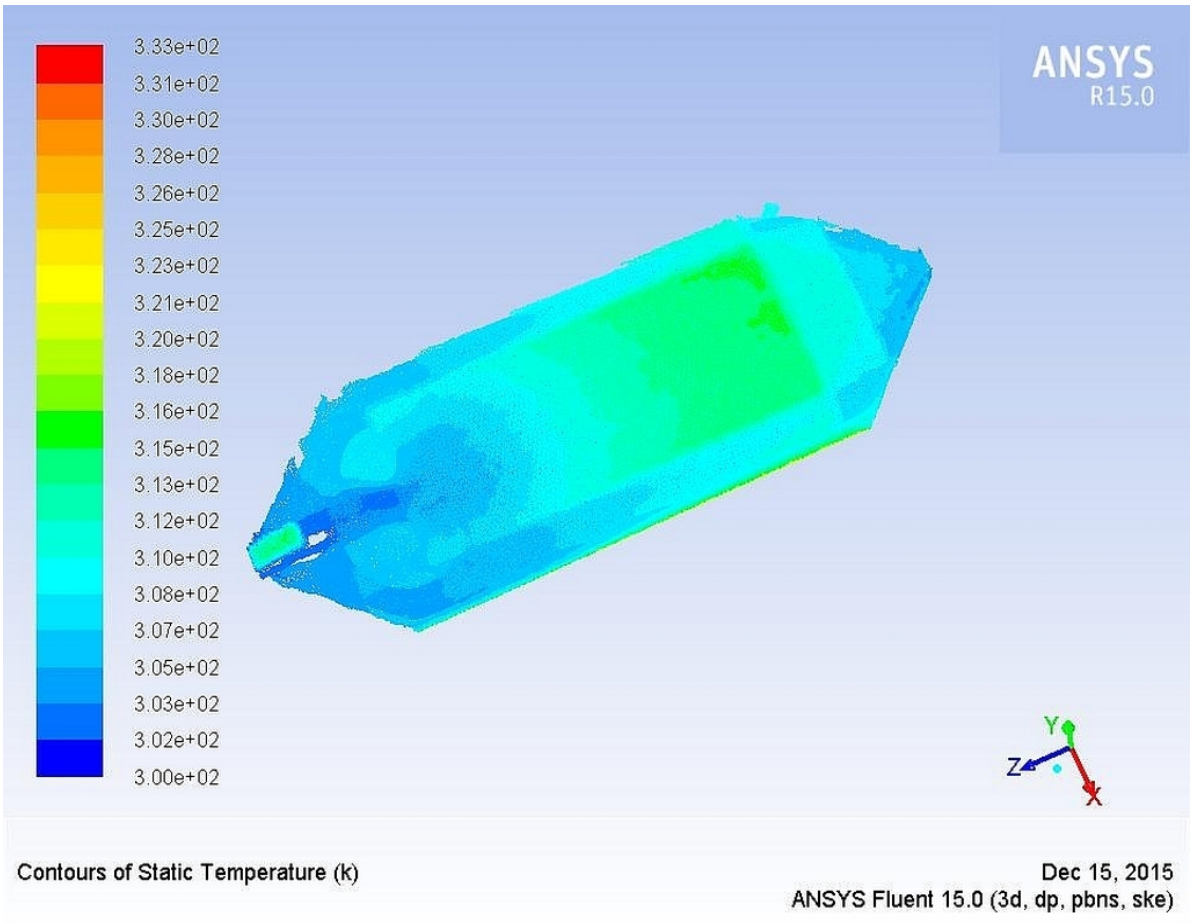

Fig 3.8: Temperature distribution with inlet □□ □□c □□ □cm/s.

The temperature profile depicted with this simulation gives us understanding of impact of velocity of temperature rise depicted with simple energy equation and turbulence model with constant heat flux conditions.

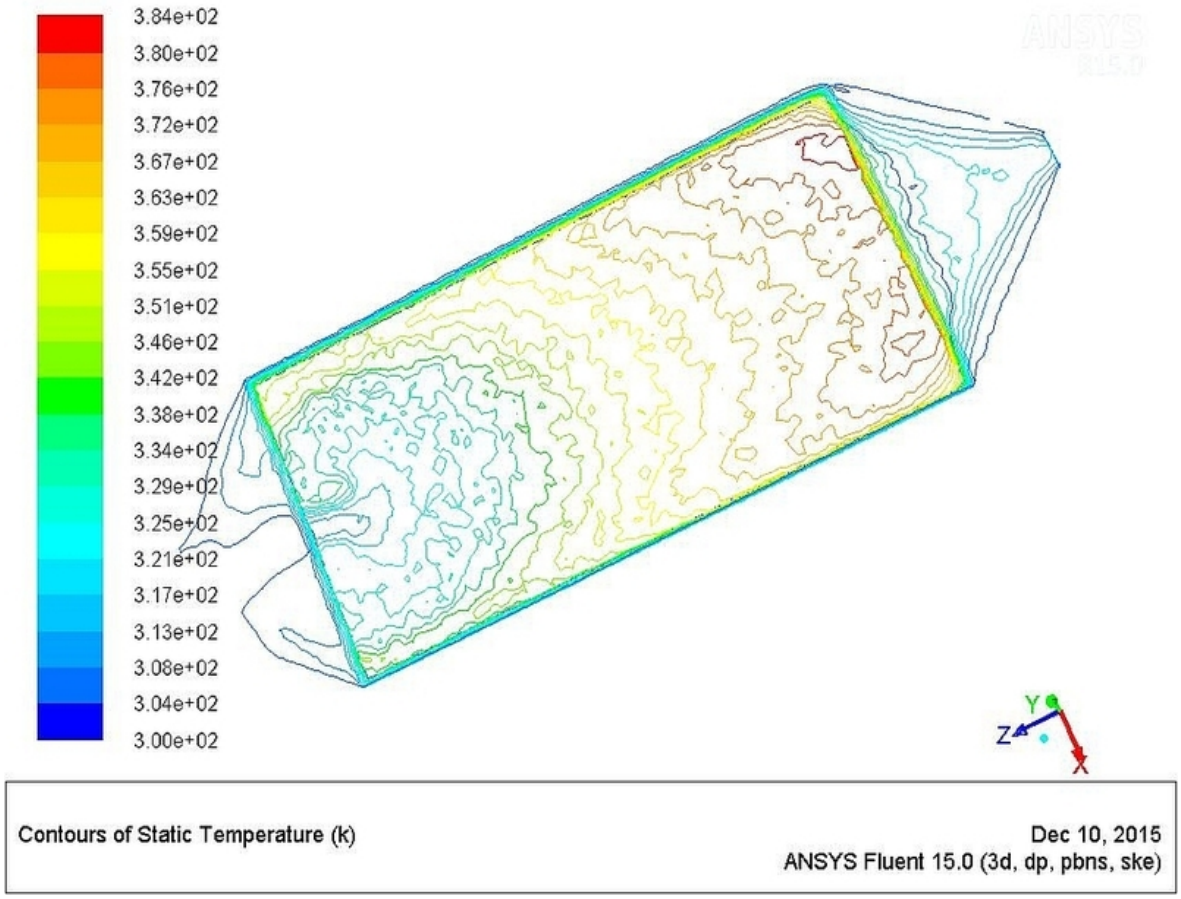

Fig 3.9: Temperature profile with □□cm/s air velocity.

Temperature distribution regarding copper as absorber plate indicating temperature difference could up to 60 K during hot summer days at peak time of day with maximum irradiation/m^2.

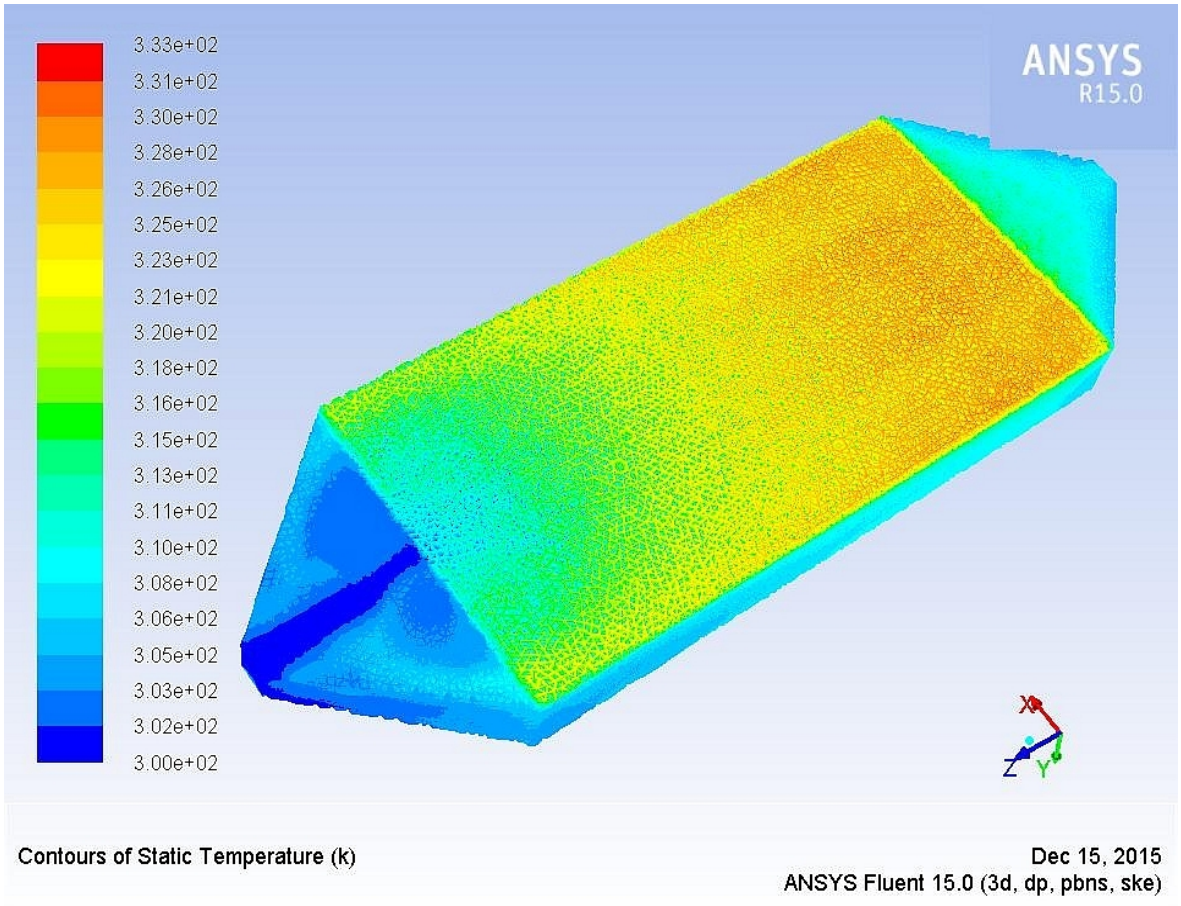

Fig 3.10: Temperature distribution with inlet □□□c□□□□cm/s (DTSR model on).

More accurate results when radiation model is incorporated while simulating conditions of air inside the solar air heater.

4.4 Theoretical Analysis

The theoretical assessment of the-solar air heater is explained in this topic. The amount of energy absorbed by the solar air heater to heat up the air and amount of energy is bombarded on it by sun. Thermo-hydraulic efficiency is also been considered; the amount of power withdrawn by the DC fan to maintain the mass flow rate of air inside solar air heater.

The angle of refraction, as the sun rays passes through air to glass cover, is calculated by Snell' law as:

$$\theta rf1 = \sin^{-1}\left[(2/3)\sin\theta i\right]$$

Similarly, the angle of refraction, as the sun rays passes through air to water, is determined as given below:

$$\theta rf\,2 = \sin^{-1}[(1/1.33)\sin\theta i\,]$$

Where θi is the incidence angle. The incidence angle is equal to the zenith angle which is defined as:

$$\theta z = \cos^{-1}[\cos(\delta_d)\cos(\varphi)\cos(\theta_h) + \sin(\delta_d)\sin(\varphi)]$$

Where δ_d is declination angle, φ is latitude angle, θ_h is hour angle.

The declination angle (δ_d) is defined as:

$$\delta_d = 23.45\left(\frac{360(284+n)}{360.25}\right)$$

Where n is the day of the year.

Hour angle (θ_h) is defined in degrees as:

θ_h = (h-12).15, where h is the local solar time, $1 \le h \le 24$.

Thermal performance of solar air heater can be expressed as fraction of energy used to raise temperature of air to the solar energy incidented. It is expressed as

Q_{useful}=m.cp.(T_o - T_{in}) where T_0 = Air temperature at exit and T_{in} = Air temperature at inlet.

The value of heat transfer coefficient (h) be increased by active and passive improving techniques. It is represented in non-dimensional form of Nusselt number (Nu).

Where $N_u = \left(\frac{hl}{k} \right)$.

Hydraulic performance = Hydraulic performance of solar air heater concerns pressure drop (ΔP) in duct of solar air heater. Pressure drop accounts energy consumption by blower to propel air through duct. Pressure drop can be represented in a non-dimensional form using following relationship of fanning friction factor (f).

f= $\Delta PD / 2\rho Lv^2$.

Cortes and Piacentini (1990) have suggested a term indicating the thermo-hydraulic performance of a flat plate solar air heater and termed it as effective efficiency.

$n_{eff} = \left(q_u - \frac{P_m}{C} \right) / I_b.A_b$ Where I_b is solar irradiance and A_b is area of absorber plate.

P_m is mechanical energy consumed for propelling air through collector and C is the conversion efficiency (mechanical power to thermal), considering that mechanical power is obtained from a typical thermal power plant and it is given by

$$C = n_{th}.n_{tr}.n_m.n_p$$

The value of C is taken by considering typical values of various efficiencies as 0.2.

n_{th} = 0.34, Thermal power plant efficiency.

n_{tr} = 0.90, Transmission efficiency.

n_m = 0.9, Motor efficiency.

n_p = 0.75, Efficiency of the pump

Instantaneous efficiency = $\left(\frac{m.c_p.\Delta T}{I_b.A_b} \right)$.

$\overline{Nu} = \overline{St} \operatorname{Re} \operatorname{Pr}$ it gives the average Nusselt number in solar air heater.

Where $\overline{St} = \left(\frac{\overline{f}/2}{1+\sqrt{\frac{f}{2}}\left\{ 4.5(e^{+})^{0.28} pr^{0.57} - 0.95\left(\frac{p}{e} \right)^{0.53} \right\}} \right)$

$$f = \left(\frac{(W+2B) f_s + W f_r}{2(W+B)} \right)$$

f_r is friction corresponding to roughened duct and f_s is friction to smooth duct.

$$f_r = \left(\frac{2}{\left[0.95\left(\frac{p}{e} \right)^{0.58} + 2.5 \ln\left(\frac{D}{2e} \right) - 3.75 \right]^2} \right).$$

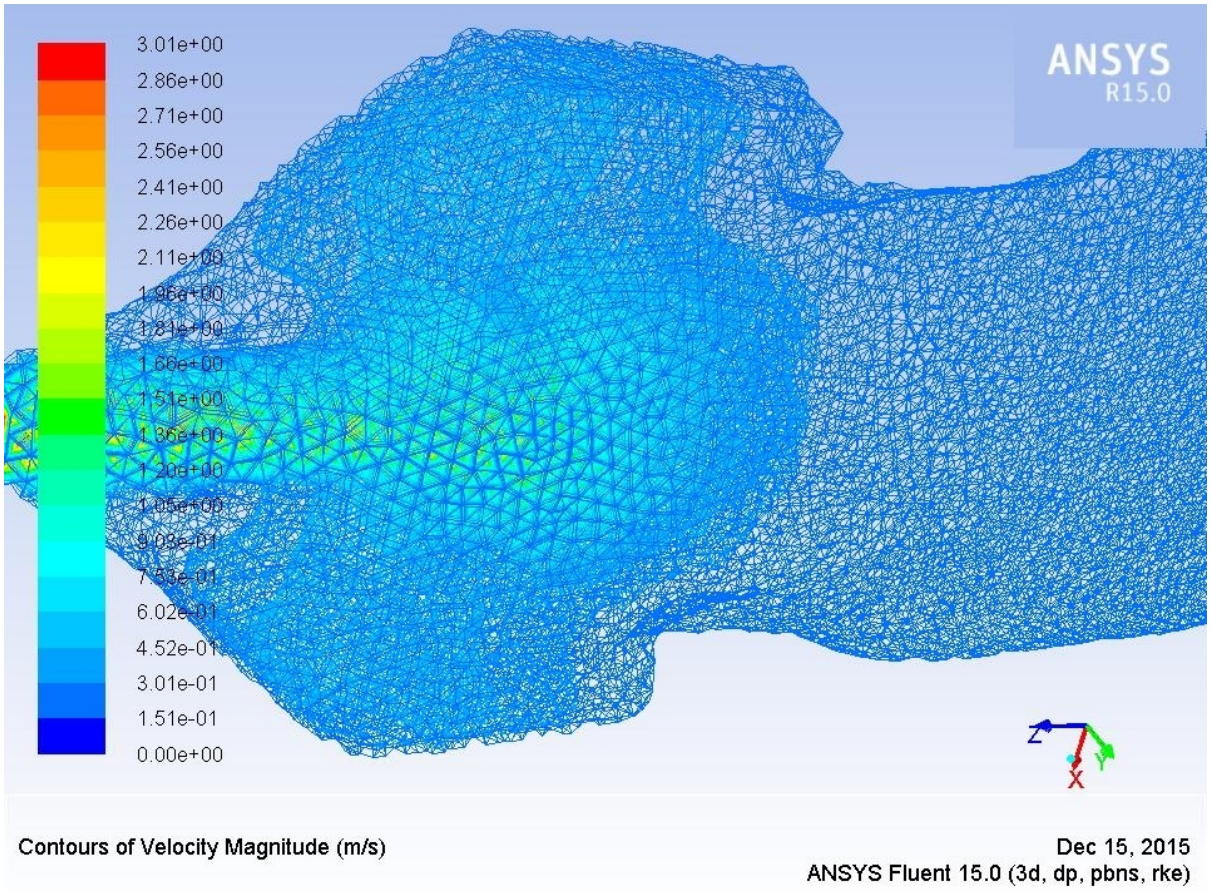

Fig 3.11: Velocity distribution over the absorber plate.

Increase in velocity is because of the increase in enthalpy of because of its rising temperature and pressure during in contact with absorber plate.

3.3 Findings from CFD modeling

- Discrete Transfer Solar Radiation model gives robust predictions on the temperature variation of the air inside Solar Air flat plate Collector.

- Corrugation is given on the Absorber plate so as to increase the air molecules turbulence; k-ε model predicts the Air motion with moderate tolerance.

- Solar ray tracing when is included gives commendable depiction of the temperature profile followed by inside solar air heater.

References

1. Selmi, M. et al. 2008. Validation of CFD simulation for flat plate solar energy collector. *Renewable Energy*. 33, 3 (2008), 383–387.
2. Luna, D., Jannot, Y., and Nadeau, J.-P. An oriented-design simplified model for the efficiency of a flat plate solar air collector. *Applied Thermal Engineering 30*, 17-18 (2010), 2808–2814.
3. Nasrin, R. and Alim, M.A. Semi-empirical relation for forced convective analysis through a solar collector. *Solar Energy 105*, (2014), 455–467.
4. Badescu, V. Optimum fin geometry in flat plate solar collector systems. *Energy Conversion and Management 47*, 15-16 (2006), 2397–2413.
5. Gómez, M.A. et al. 2013. CFD simulation of a solar radiation absorber. *International Journal of Heat and Mass Transfer*. 57, 1 (2013), 231–240.
6. Ekechukwu, O., Heinzel, V., and Gordeev, S. CFD analysis of a thermo-hydraulic flow distribution in generic indirect-type natural-circulation solar-energy dryers. *International Journal of Sustainable Energy 33*, 1 (2012), 159–178.
7. Sumathy, K., Venkatesh, A., and Sriramulu, V. Heat-transfer analysis of a flat-plate collector in a solar thermal pump. *Energy 19*, 9 (1994), 983–991.

Chapter 4

Experimental setup and procedure

4.1 Description of experimental setup

The sole purpose of this experimental was to setup an efficient solar air heater. The solar air heater is used to dry spices , vegetables, fruits, and many more other objects which need moisture control to avoid addling. The solar air heater is 1m in length and is 1m wide. The absorbing area of the air heater is 1.1177m^2. Solar air heater is constructed at Thapar University in Patiala, India (30.3568° N latitude, 76.3688° E longitude). The top of the air heater is covered with double glass cover to minimize the radiation losses. The bottom covering of the solar air heater is insulated with expanded polystyrene sheets of 25mm thickness to minimize conduction as well convection losses. The absorbing section of the air heater is made of stainless steel (204 grades) and is painted with dull black board colour to increase its absorptivity. Higher the absorptivity, higher will be the temperature of the plate and higher will be the heat flow from absorbing plate to the working fluid (Air).

First, the materials are procured for making the solar air heater. The frame of the solar heater which takes the weight of the device is made from iron angles of 0.75inch width and 32 feet in length. The frame is made and the stainless steel sheet after bending it in mechanical press is moved in the frame. The absorbing plate and glass cover rests on the iron frame. Glazed iron sheets are used to make the bottom plate of the solar air heater and its side walls and solar heaters inlet as well outlet section. Glazed sheet of 12*8 feet size was used as per design considerations. The glasses used at top have transmissivity of 0.95. Two glasses have a gap of 5 mm in between them to curb the conduction losses by top glass cover. The stand which is inclined as per inclination angle specific to place is made from iron angles of 0.75inch width to cope-up with the weight of the setup. The mirrors used to make the

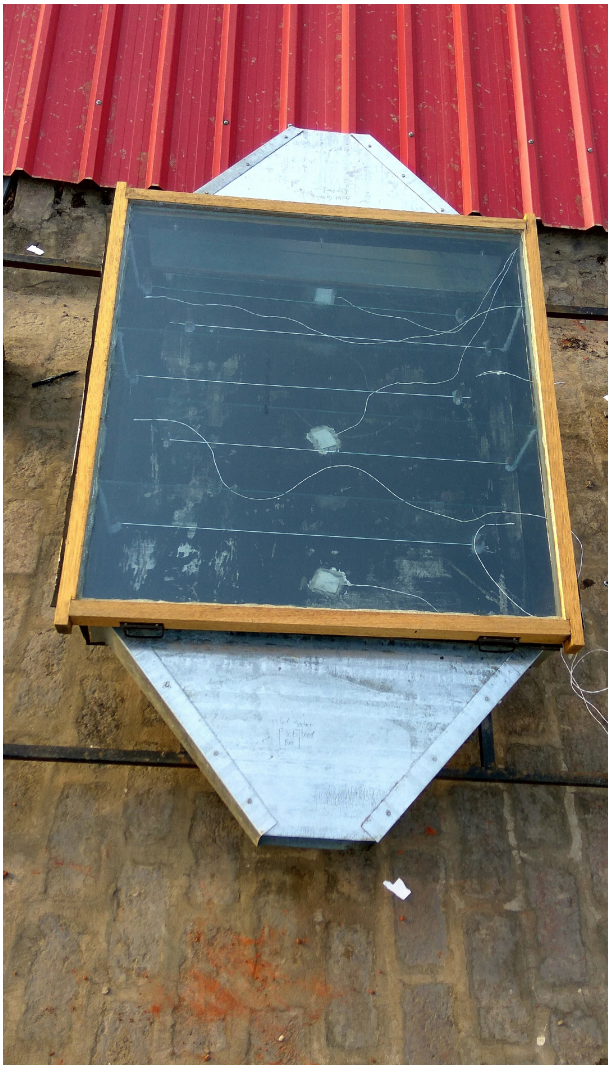

Fig 4.1: Solar air heater with multi-pass adjustment.

The setup is tilted as per inclination angle suitable to the location (Patiala). The inlet and outlet sections are made of such type so as to give relaxation to air so that it could flow all over the absorber plate. The temperature profiles of air are recorded with an Arduino board compatible with t-type thermocouples. Readings were taken from 10 AM to 3 PM in some cases were taken up to 5 PM.

4.2 Fabrication of solar air heater

The walls of the inlet and outlet cover are made from glazed iron sheets. The sheets were of 26 gauze thickness and walls are of near 400mm. Height of the walls is equal the depth of the solar air heater. The walls are little rugged because of the daily wear during handling.

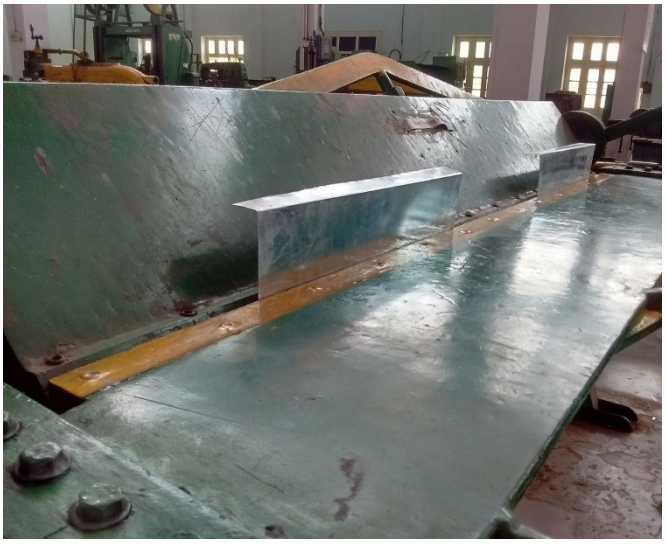

Fig 4.2: Inlet & Outlet cover walls bending.

The walls of outlet and inlet cover after being pressed in a mechanical press machine. The angle of bend is 90 degrees.

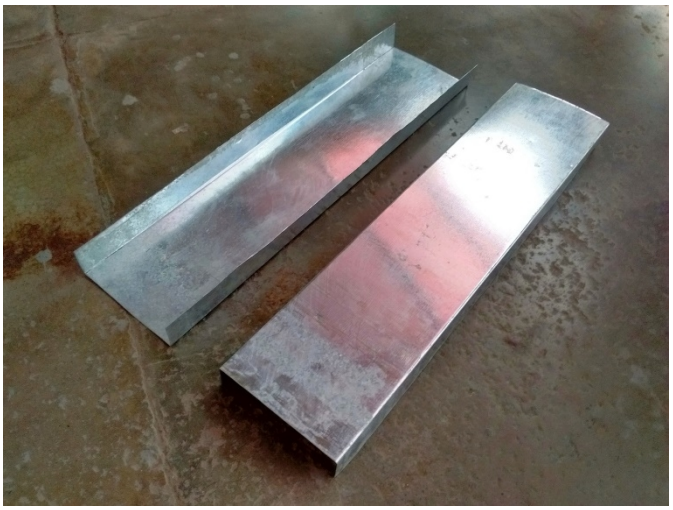

Fig 4.3: Inlet and outlet cover of walls after bend.

Inlet cover of the solar air heater. It allows air inside the experimental setup. It is cut out from glazed iron sheets. The thickness of the sheet is enough to support the weight of the whole cover hence no support is given to inlet and outlet cover of solar sir heater.

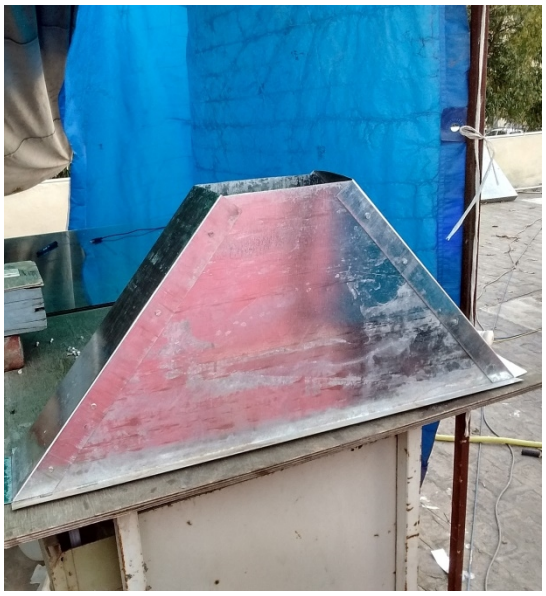

Fig 4.4: Inlet cover of the solar air heater.

Inside of the inlet/Outlet cover. This is further attached with the main body of the solar air heater. Riveting i□done to make the joining of the sheets leak proof. In addition sealants are like silica gel and rubber sheet is used to leak proof the joints.

Fig 4.4: Inside view of covers.

The bottom plate of the solar air heater is filled with insulating material; EP sheet to minimize the conduction losses.

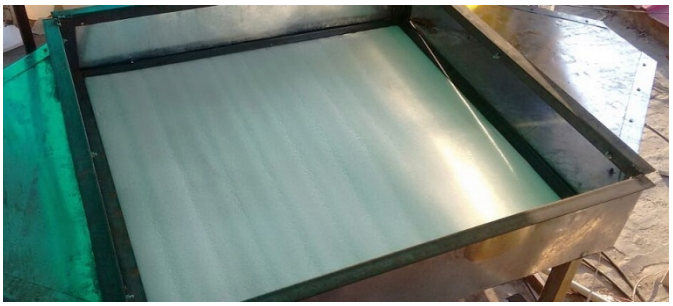

Fig 4.5: Insulating the rear of solar air heater.

The stainless sheet after paint has dried over it is placed inside the solar air heater. Solar air heater if further placed on the iron stand to adjust as per the declination angle of the location. For controlling the mass flow rate inside the solar air heater a DC fan is also installed at the mouth of the collector.

Fig 4.6: Absorber and Insulation installed in collector.

Double glass cover lowers the radiation losses inside the solar air heater. It has transmissivity of 0.95. It allows the shortwave length radiation to enter through it while it does not allow long wave length radiation which is emitted by absorber to go through it.

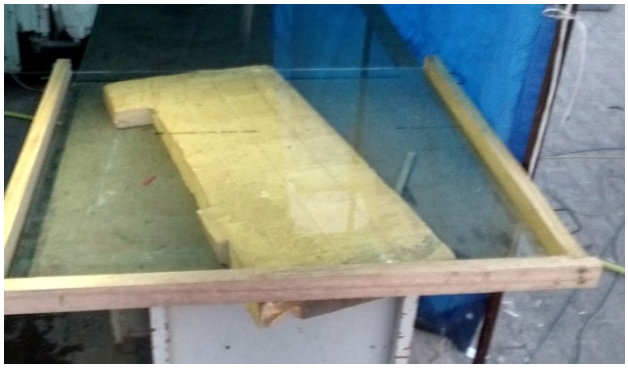

Fig 4.7: Double glass cover of solar air heater.

Double glass cover placed on the solar air heater with thermocouples attached to test the temperature readings of the display board. The whole assembly rests on the iron stand which is inclined ranging 15-30⌈ depending upon day of the year and location of the place.

The outlet of the solar air heater is choked so as to restrict air from surrounding to enter the air heater from outlet cover opening on a windy day. The solar heater is inclined to assist the flow of air as hot air rises up due to density difference.

Fig 4.8: Solar air heater with double glass covers on.

Fig 4.9: Variable speed fan for controlling air mass flow inside solar air heater.

Fan is a 12V powered DC fan whose RPM can be controlled by connecting it with a rotary switch containing different ohm resistors to manipulate speed as per requirement. The fan speed could go from 0.8 to 5 m/s.

Fig 4.10: Multi-Pass arrangement on absorber plate.

The multi-passing is done with mirrors only. Multi-passing with metal sheet is avoided as it introduces shading on the metal absorber plate which affects the performance of the solar air heater. The glass strips allow all sun rays to hit the absorber plate and does not introduces shading on the absorber plate. Air contact with metal sheet is sacrificed in order to curb the shading losses.

4.3 Instrumentation and measurement

Temperature readings were taken with 9 pt-100 temperature sensors accurate with range of ±0.5⌈C. The radiation intensity is measured with pyranometer. The thermocouples could determine temperature from -50⌈C to 200⌈C with ease and minimum error. The thermocouples are placed on absorber sheet and 5 are hung in air by attaching them with mirror placed on absorber section.

Distance between the thermocouples is equal on the absorber plate while the thermocouples which are hung in air are placed at irregular distances corresponding to the channels made on the absorber plate.

The intensity of solar radiations is measured with the help of Pyranometer. Pyranometer measures the direct solar beam and diffused radiations coming from the sun. This pyranometer takes the reading after every 10 minutes and data logger is attached which is further connected to the computer to log the values of solar intensity. The pyranometer by Kipp & Zonen (CMP 11) is used with operational irradiance 4000 W/m^2. Operating and storage temperature range 40 °C to +80 °C and Sensitivity 7 to 14µV/W/m^2.

Fig 4.11: Pyranometer.

The board is compatible with the p-type thermocouples. The maximum capacity of thermocouples which can be installed in it is 10. The resistance offered is less as found from thermocouples calibration thus the actual temperature result is not much affected.

Fig 4.12: Arduino board displaying temperature, Flow rate and RPM display.

Velocity meter was used to gauze the velocity of the variable speed fan. Accurate up to ± 0.3m/s. The fan is made to rotate just next variable speed fan r□□ □□□c□□□□r□d□□□□□□□r□□□□d□□□□□r□□□ displayed on the screen of the instrument.

Fig 4.13: Speedometer.

Table 4.1: Calibration data for temperature sensors (all values are in °C).

Thermometer readings	T_1	T_2	T_3	T_4	T_5	T_6	T_7	T_8	T_9
21	19.6	20.4	21.3	21.5	22.4	23.1	21.4	22.2	21.5
26	26.7	25.5	25	24.8	27.5	26.4	27.1	27	25
29	30	30.1	29.5	29.1	29.4	30.5	28.7	28.4	29.9
35.5	35.4	34.8	35.5	35	35.9	34.5	34.9	35.4	36
42	43.1	42.7	42.6	42.3	41.4	41.6	43.1	42.8	41.9
47	48.4	47	46.1	46.5	47.5	48.1	47.5	47.1	47.2
51	52	51.7	52.1	51.1	50.1	49.9	50.9	51.4	52.1
54	54.9	55	54.1	53.1	53.5	55.1	55.2	53.8	54
60	59.6	60.4	61.2	60.8	60.3	58.8	59.5	59	60.3

Table 4.2: Properties of air at 1 atmospheric pressure.

Temperature (°C)	Density (kg/m^3)	Specific heat (c_p) (J/kg.K)	Thermal conductivity (k) (W/m.K)	Dynamic Viscosity (kg/m.s)	Prandtl number (Pr)
0	1.292	1006	0.02364	1.179	0.7362
5	1.269	1006	0.02401	1.754	0.7350
10	1.246	1006	0.02439	1.778	0.7336
15	1.225	1007	0.02476	1.802	0.7323
20	1.204	1007	0.02514	1.825	0.7309
25	1.184	1007	0.02551	1.849	0.7296
30	1.164	1007	0.02588	1.872	0.7282
35	1.145	1007	0.02625	1.895	0.7268
40	1.127	1007	0.02662	1.918	0.7255
45	1.109	1007	0.02699	1.941	0.7241
50	1.092	1007	0.02735	1.963	0.7228
60	1.059	1007	0.02808	2.008	0.7202
70	1.028	1007	0.02881	2.052	0.7177
80	0.9994	1008	0.02953	2.096	0.7154

Chapter 5

Results and Discussions

Experiments were performed on solar air heater and temperature readings were recorded with RTD (Resistance Temperature Detector) Pt-100 sensors. Temperature profiles were recorded on natural convection mode, forced convection mode, natural convection multi-pass mode, forced convection multi-pass mode and forced convection induced turbulence mode. The data were taken in month of May and June because of less incidence angle of irradiation.

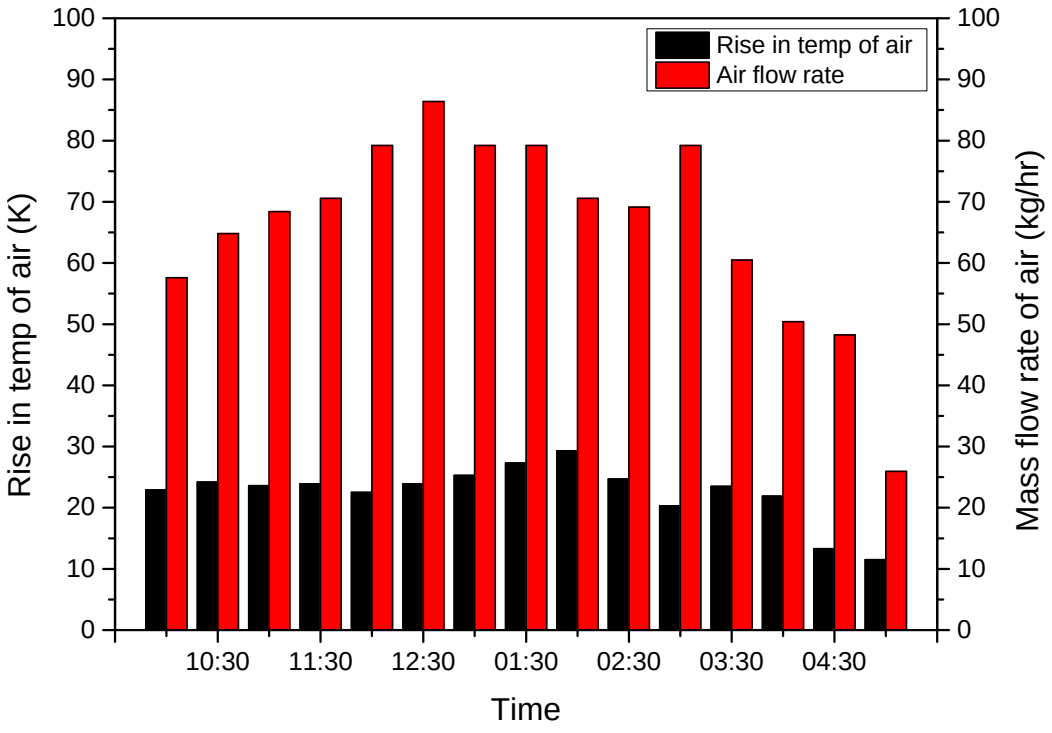

Fig 5.1: Mass flow rate and Temperature profile of air in Natural convection mode on 14/05/2016.

The graph in fig 5.1 shows the variation in mass flow rate and Air temperature rise in a solar air heater in natural convection mode during the day. The rise in mass flow rate of air in graph is because during 12 NOON to 3 PM the air temperature is maximum and pressure

drop is maximum inside solar air heater leading to maximum suction of air due to natural convection.

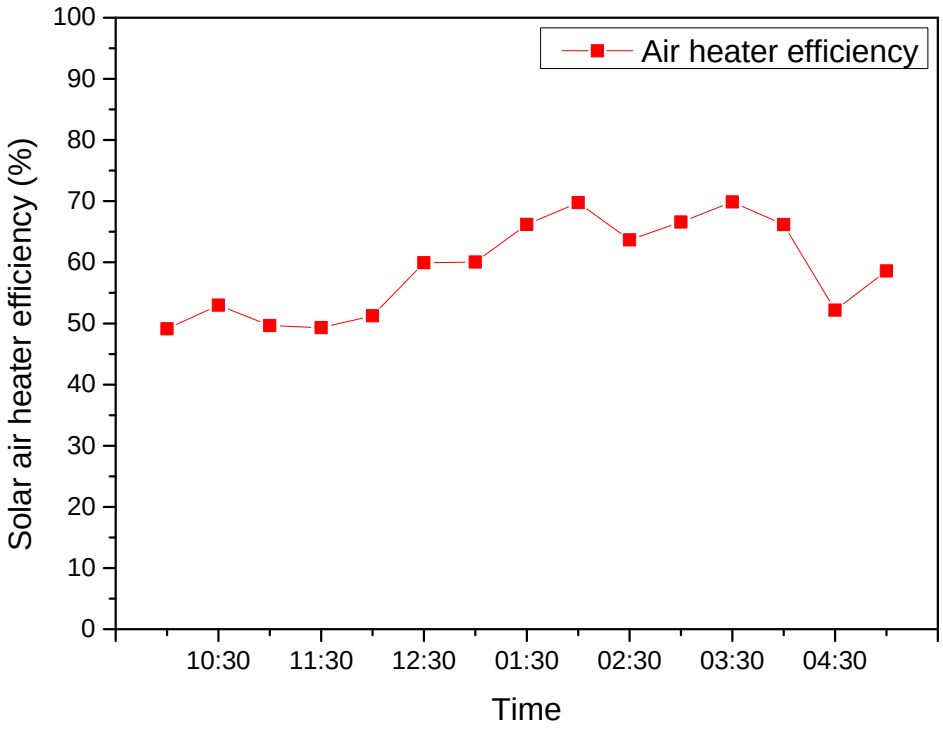

Fig 5.2: Solar air heater efficiency in natural convection mode of air on 14/5/2016.

The graph ion fig 5.2 depicts the profile of collector efficiency in natural convection mode of air inside solar air heater. Maximum efficiency is achieved at 12 NOON to 3 PM during the day because of high irradiation and correspondingly higher heat transfer rate from absorber plate to the working fluid.

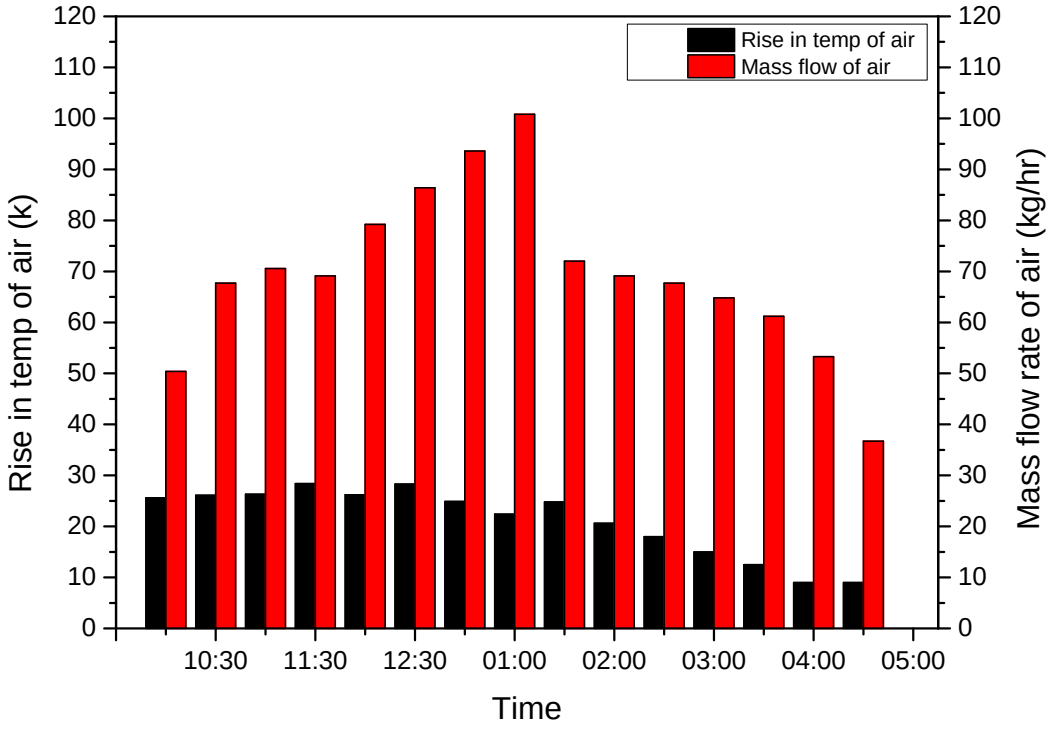

Fig 5.3: Mass flow rate and Air temperature profile of solar air heater in natural convection mode of air on 15/5/2016.

Peak flow rate and culmination of rise in temperature of air insinuates the maximum efficiency would also be achieved during this time of the day corresponding to the zenith values in irradiation.

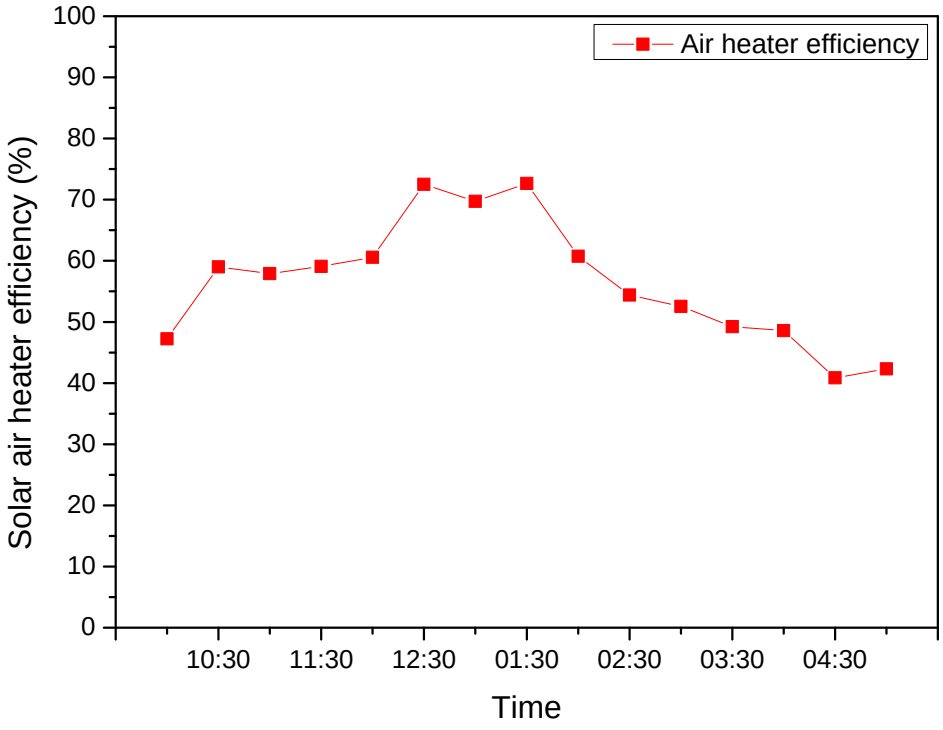

Fig 5.4: Solar air heater efficiency with natural convection mode of air on 15/05/2016.

Collector efficiency variation during the daytime on 15/05/2016 is shown in the graph represented by fig 5.4. Maximum efficiencies are achieved during peak irradiation hours of the day.

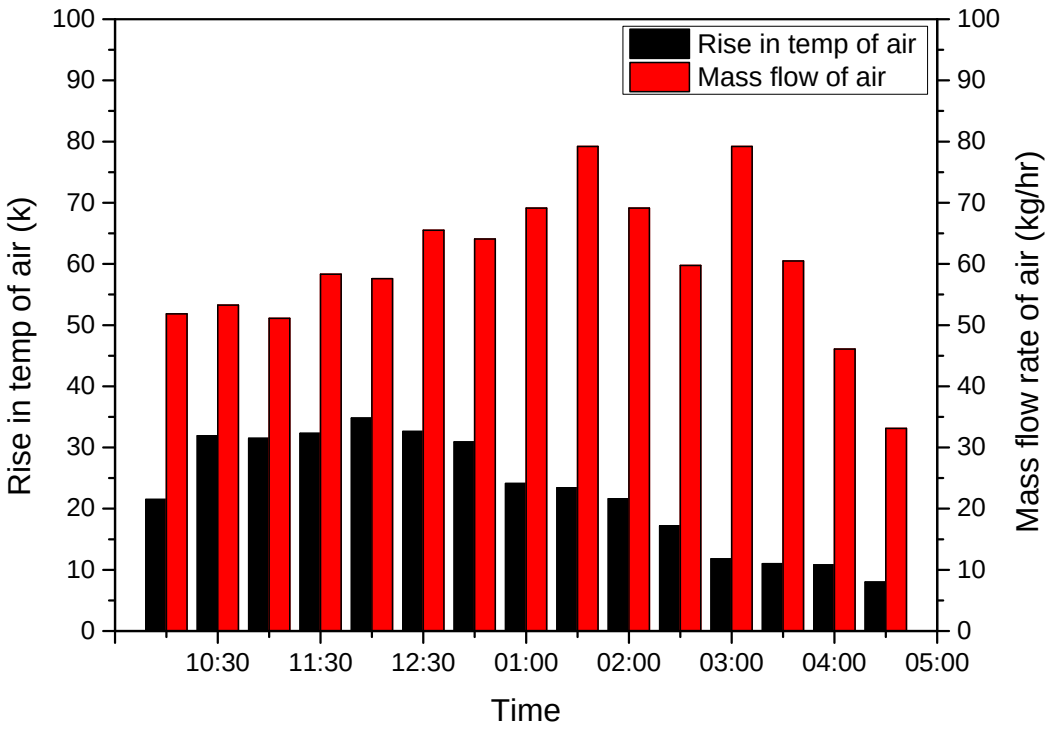

Fig 5.5: Mass flow rate and Air temperature profile corresponding to natural convection mode of air inside solar air heater with multi-passing on 05/06/2016.

The variation in mass flow rates in the fig 5.5 is because of the performance of solar air heater depends on the mercy of weather. Windy, Hazy, Cloudy day affects the sola air heater efficiency profusely.

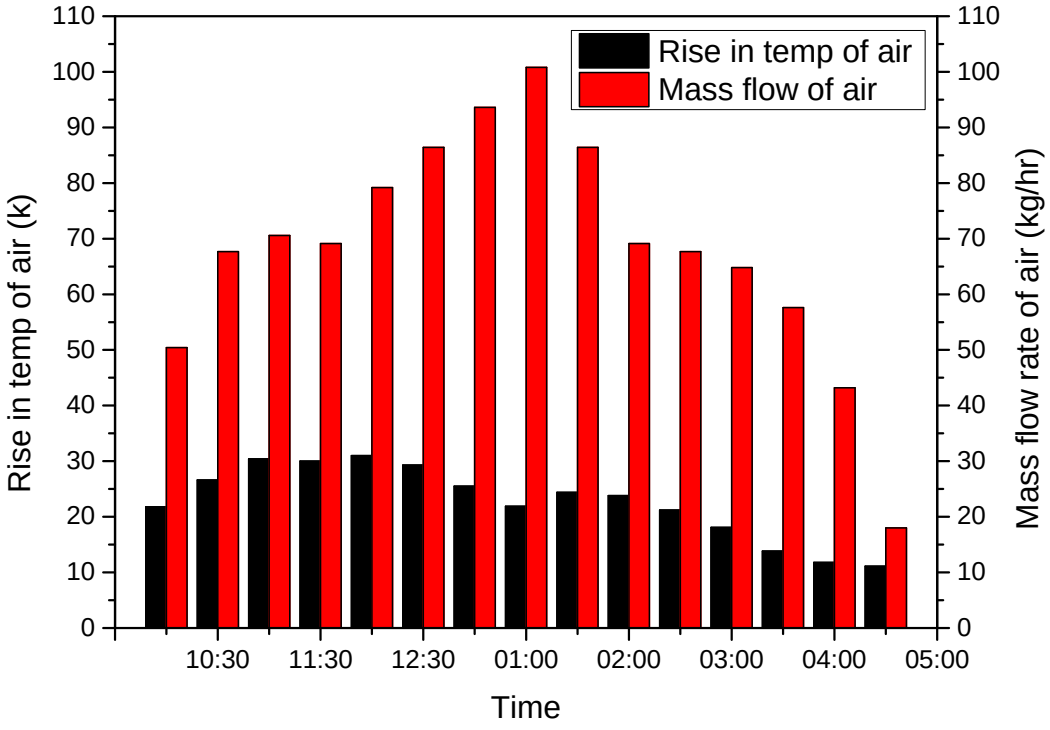

Fig 5.6: Mass flow rate and Air temperature rise in solar air heater in Natural convection mode of air with multi-passing on 27/05/2016.

The rise in efficiency in this adjustment compared to natural convection mode but with single pass inside solar air collector is because air residence time has increased thereby more heat transfer is possible to the air from absorber plate. Mirrors used to make the multi-pass arrangement do not cast any shadow on absorber plate thus performance of solar air heater is augmented instead of deterioration.

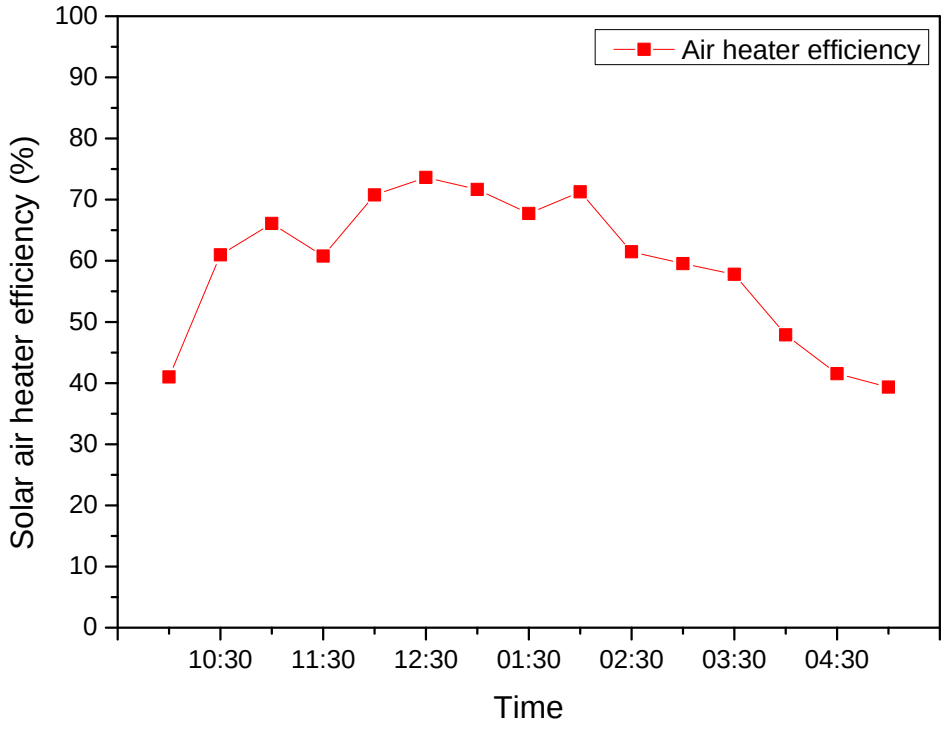

Fig 5.7: Collector efficiency of solar air heater with natural convection of air and multi-pass of air over absorber plate on 27/05/2016.

The graph in fig 5.7 shows variation of efficiency of solar air collector on 27/05/2016. Efficiency of solar air heater is more relaxed in when multi-pass is done over absorber plate thus indicating higher air temperatures when air leaves the solar air heater. Mass flow rate of air vary with temperature of air achieved inside solar air heater. Higher the temperature achieved higher will be the pressure drop across the solar heater leading to more suction of air from inlet.

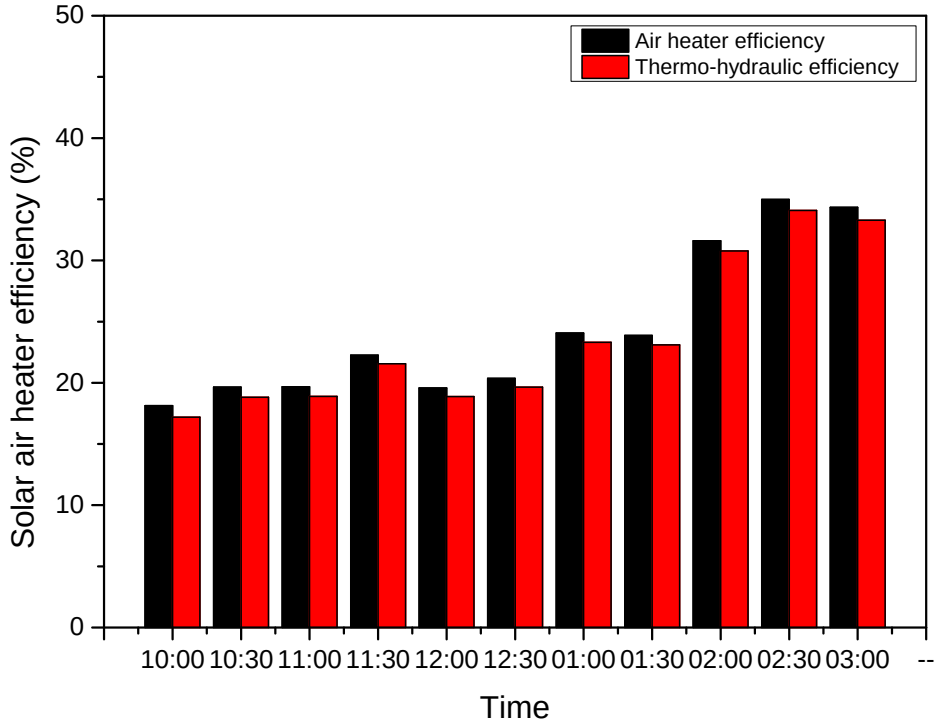

Fig 5.8: Collector and Thermo-hydraulic efficiency of solar air heater with constant mass flow rate of 36.144 kg/hr and forced convection mode on 08/06/2016.

The thermo-hydraulic efficiency given by fig 5.8 is less than collector efficiency because it is the net effective efficiency; Useful energy picked by air heater Energy consumed by DC fan. Thermo-hydraulic efficiency bears a direct relation with the pressure drop across solar air heater.

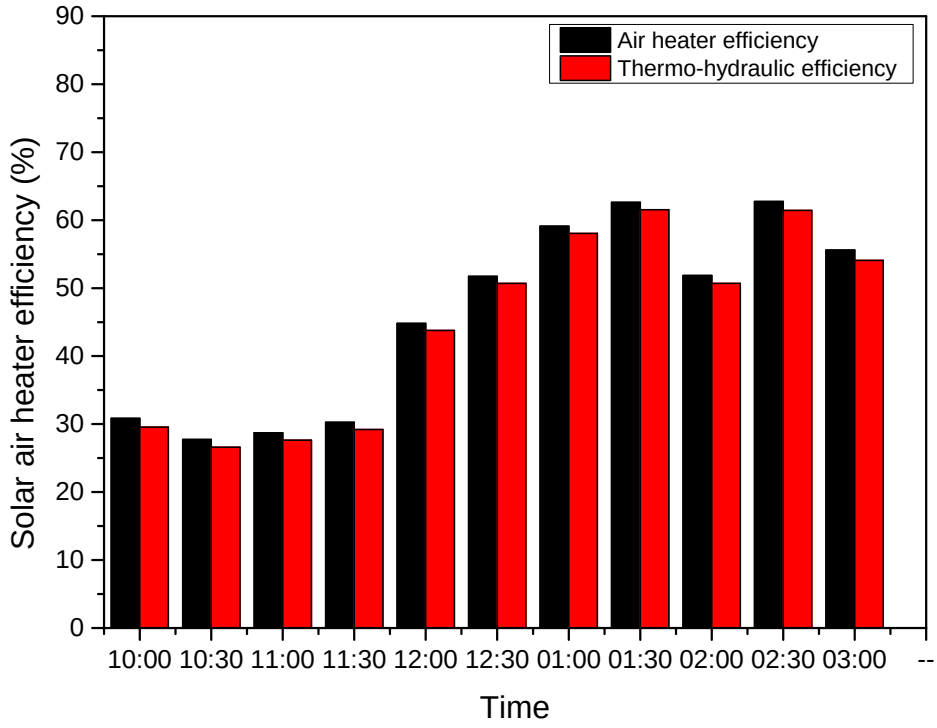

Fig 5.9: Collector and Thermo-hydraulic efficiency of solar air heater with constant mass flow rate of 54.216 kg/hr and forced convection mode of air on 09/06/2016.

With increased mass flow rate corresponding to peak irradiation hours during day Fig 5.9 shows variation of efficiency of solar air heater. Thermo-hydraulic efficiency power is evaluated by P=V*I where V=Voltage supplied to fan from rotary switch and I= Current given to fan.

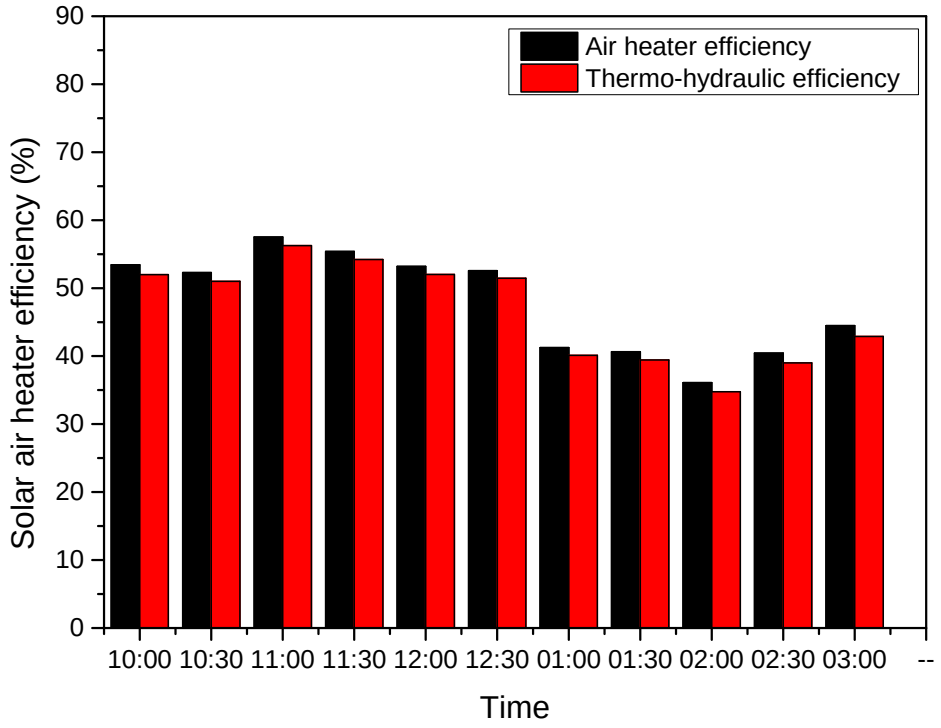

Fig 5.10: Collector and Thermo-hydraulic efficiency of solar air heater with constant mass flow rate of 72.288 kg/hr and forced convection mode of air on 10/06/2016.

Mass flow rate is highest in such configuration of solar air heater with multi-pass over the absorber plate. Power consumed by fan is also considerable given the time of operating hours it plays a major role in the deciding of whether external media for thermal performance enhancement be used or not. The configurations has been adjusted with multi-pass, forced convection and turbulence induced with external wires twisted in form of coil to induce swirling motion of air.

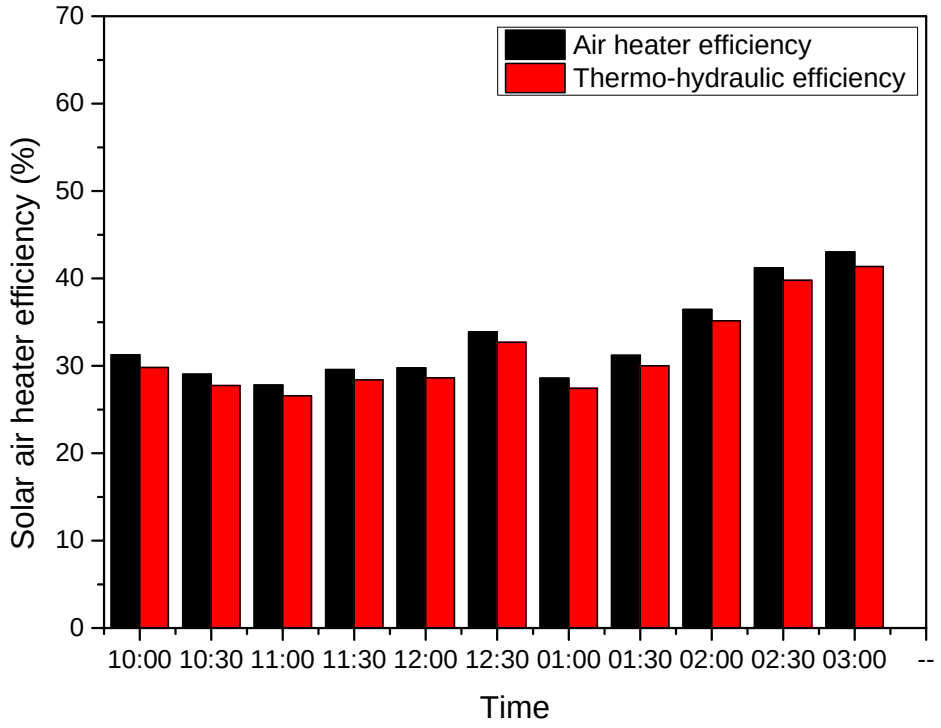

Fig 5.11: Solar air heater efficiency in forced convection mode with multi-pass of air with constant mass flow rate of 36.144 kg/hr with induced turbulence in form of coiled wire over absorber plate on 12/06/2016.

The coiled wires were used to induce turbulence inside the solar air heater to increase heat transfer co-efficient. Turbulence induced by wires encourages air molecules to swirl over the absorber plate analogous to swirling motion of fuels inside internal combustion engines. This swirling of air molecules facilitates more heat transfer from absorber plate to working fluid. The graph in fig 5.11 gives the variation of solar air heater efficiency in such configuration.

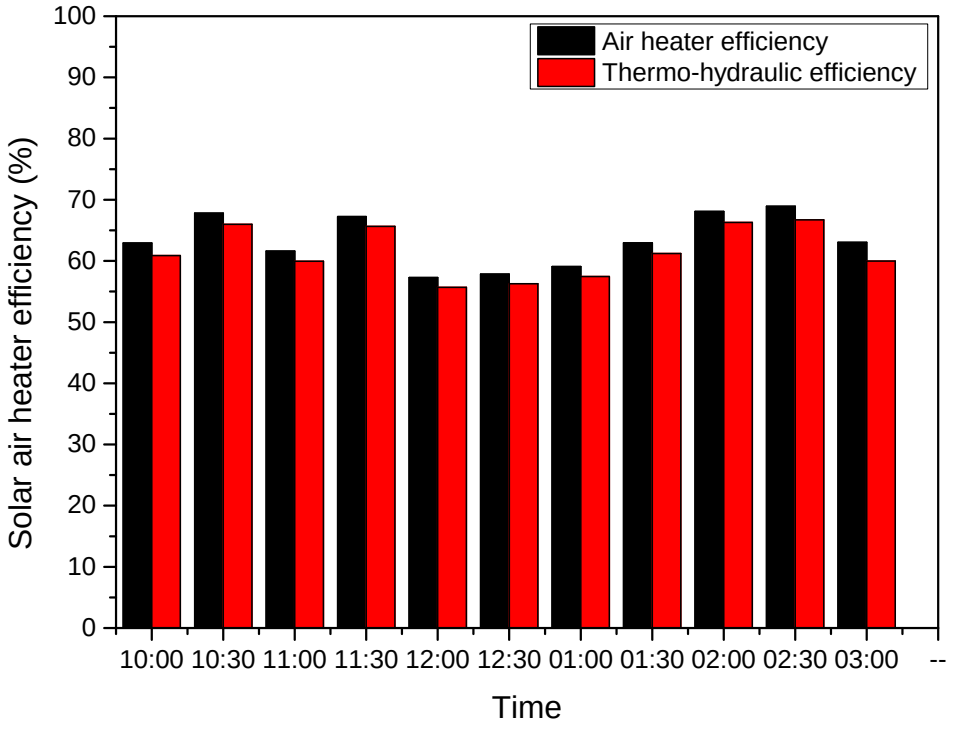

Fig 5.12: Solar air heater efficiency in forced convection mode with multi-pass of air with constant mass flow rate of 72.288 kg/hr with induced turbulence in form of coiled wire over absorber plate on 14/06/2016.

The collector efficiency pertaining to constant flow rate of 72.288 kg/hr is shown in fig 5.12. The collector efficiency shows a rising trend of efficiency because irradiation is maximum in month of June. $Q_{useful} = \dot{m}.cp.\zeta T$ Where $\dot{m}$ is mass flow rate. Here mass flow is apposite to the irradiation available and as per design of solar air heater. This configuration is run at □□ cm/s of inlet speed of air leading to 13 watts of power consumption only by fan.

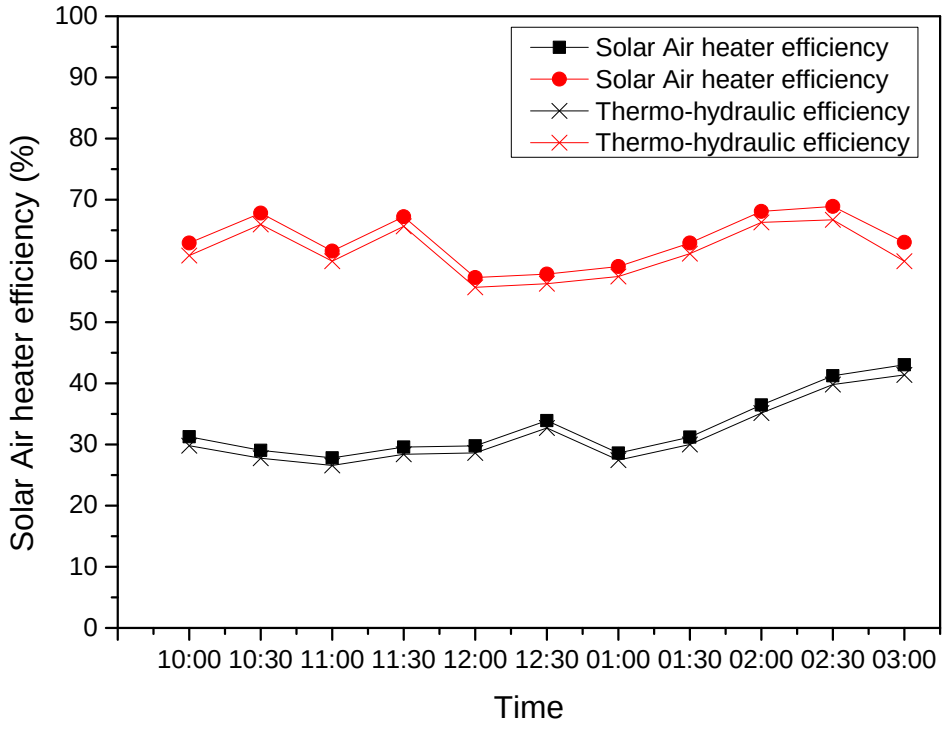

Fig 5.13: Comparison of Solar air heater efficiency and Thermo-hydraulic efficiency in forced convection mode with induced turbulence of air on 12/06/2016 and 14/06/2016.

The lines in black colour correspond to solar air heater performance on 12/06/2016 and the lines in red colour correspond to solar air heater performance on 14/06/2016. The air heater efficiency though high on 14/06/2016 it yields less rise in temperature of air pertaining to the solar air heater performance on 12/06/2016. It is because of the difference in mass flow rate of air inside solar air heater.

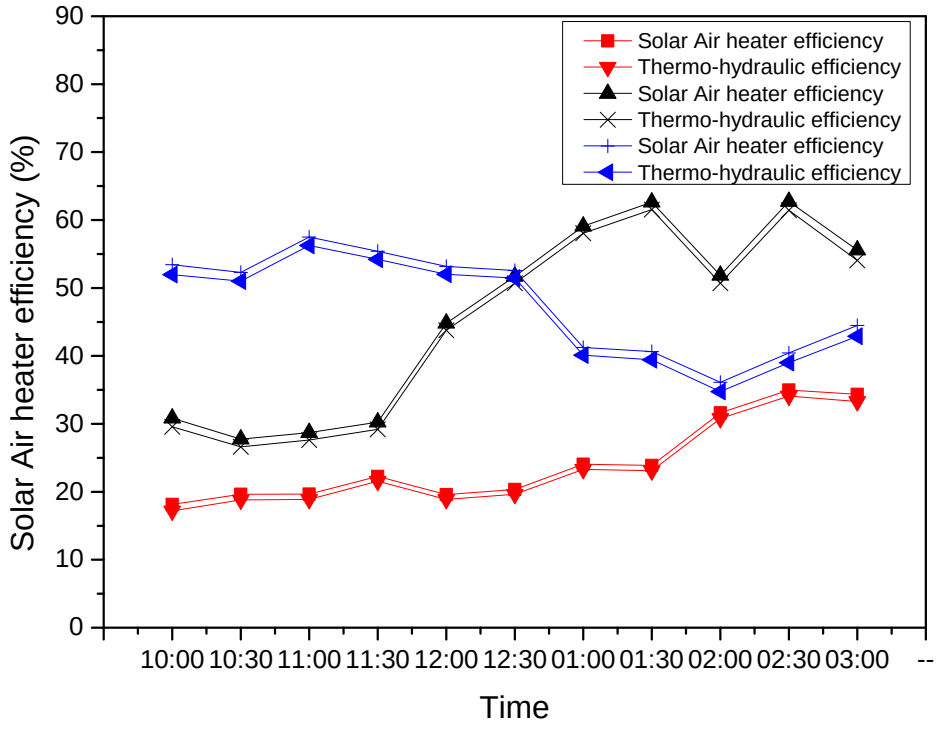

Fig 5.14: Comparison solar air heater and Thermo-hydraulic efficiency of solar air heater in forced convection mode without turbulence on 08/06/2016, 09/06/2016 and 10/06/2016.

In the fig 5.14 the blue lines represent solar air heater performance on 10/06/2016 with mass flow rate of 72.288 kg/hr and the red lines represent solar air heater performance on 09/06/2016 with mass flow rate of 54.216 kg/hr and the black lines represent solar air heater performance on 08/06/2016 with mass flow rate of 36.144 kg/hr.

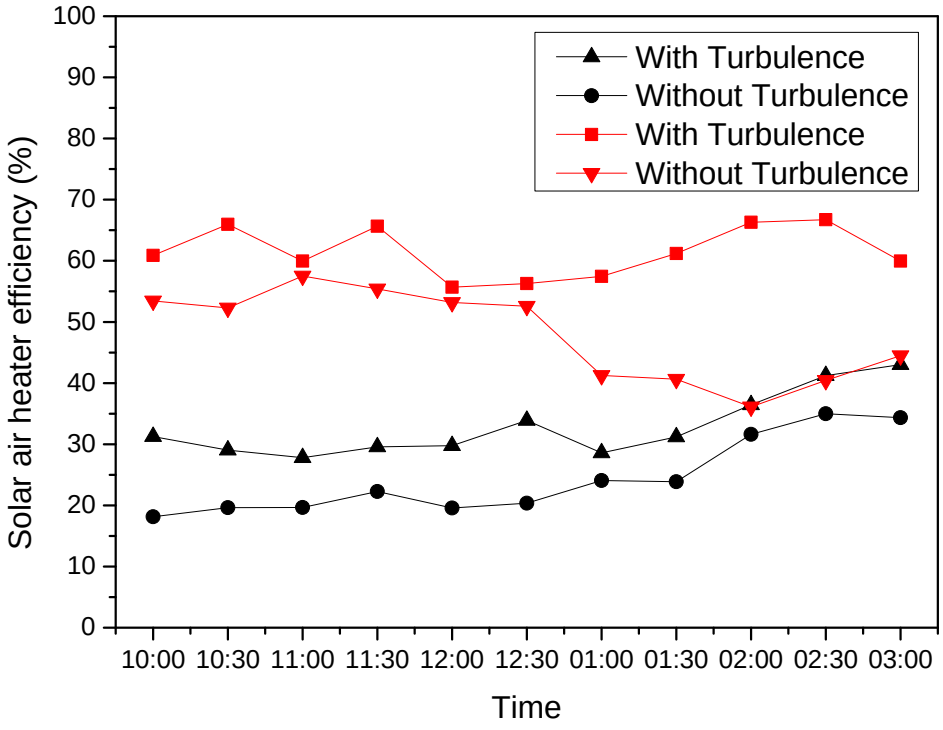

Fig 5.15: Comparison of Solar air heater efficiency with and without turbulence at mass flow rate of 36.144 kg/hr and with and without turbulence at mass flow rate of 72.288 kg/hr in forced convection mode of air.

In fig 5.15 it is shown that swirling motion induced in the solar air heater while air flowing over absorber plate results in better performance of solar air heater. The coiled wires inside solar air heater induces swirling motion in air thereby making more displacing of air molecules over the plate resulting in higher heat transfer from absorber plate to the working fluid (air). The red lines in graph are associated with mass flow rate of 72.288 kg/hr and black lines are associated with mass flow of 36.144 kg/hr.

Chapter 6

Conclusions and Future scope

6.1 Conclusions

The following conclusions were made by undertaking the project of Air solar flat plate collector analysis with induced turbulence:

1. The Solar air heater performance in natural convection mode with multi-pass is better than the Single pass natural convection mode. It is because the residence time with multi-pass increases though the radiation losses also increase but they are curbed by double glass cover.
2. The rise in air temperature is quicker in case of multi-pass channel made with glass than in case of multi-pass channels made with metal strips. It is because the shading losses in case of glass channels are almost negligible
3. Solar air heater performance in parameters of efficiency and rise in temperature of air both are better in case with induced turbulence mode with forced convection of air with multi-pass than in case of forced convection of air without turbulence with multi-pass. There is increase of 10% to 25 % of solar air heater efficiency in induced turbulence mode.
4. Energy consumption in case of induced turbulence by DC fan is more than without turbulence case thereby affecting thermos-hydraulic efficiency of solar air heater with induced turbulence. Power consumption by Dc fan goes up to 13 watts and increases when fan speed is increased.
5. Temperature rise of air in case of induced turbulence mode with mass flow rate of 34.144 kg/hr is more than 5 ⌈C than in case with induced turbulence mode and mass flow rate of 72.288 kg/hr.

6.2 Future Scope of work

Solar air heater performance depends mainly on irradiation and amount of contact area available for air to pick up heat. External media used to increase performance of heat transfer also associates with them shading losses and pressure losses leading to more power consumption to propel air inside solar air heater. The glass used to channelize the flow inside solar air heater does not cast any shading losses.

- To induce turbulence in air, different patterns of glass material could be used and even suspended in passage of air without casting any shading on absorber plate.
- Much sophisticated material of absorber plate could be used to increase performance of solar air heater. Materials with high absorptivity increases temperature of absorber plate leading to higher heat transfer between air and absorber plate because of high temperature gradient.
- Coating of paint over absorber plate also enhances solar air heater performance. Example - Coating of material like Vantablack made of carbon nanotubes on absorber plate. The coating has ability to soak 99.965 % of radiation incidented on it.

Appendix A

Table A1: Solar air heater performance on natural convection of air without multi-pass on 14/05/2016.

Time	Mass Flow rate	Cp	□□□□□□ □ rise of air	$Q_{incidented}$	$Q_{useful\ (watts)}$	η_i (Instantaneous efficiency)
	kg/hr	J/Kg.k	K	(Watts)	$m*c_p$□□□	%
10:00 AM	57.6	1003	22.9	748.027	367.499	49.129
10:30 AM	64.8	1003	24.2	824.318	436.907	53.002
11:00 AM	68.4	1003	23.6	905.993	449.745	49.641
11:30 AM	70.56	1003	23.9	952.592	469.845	49.323
12:00 PM	79.2	1003	22.5	968.741	496.485	51.251
12:30 PM	86.4	1003	23.9	959.956	575.321	59.932
01:00 PM	79.2	1003	25.3	929.917	558.270	60.034
01:30 PM	79.2	1003	27.3	910.011	602.402	66.197
2:00 PM	70.56	1003	29.3	825.619	576.003	69.766
2:30 PM	69.12	1003	24.7	747.203	475.663	63.659
3:00 PM	79.2	1003	20.3	672.795	447.940	66.579
3:30 PM	60.48	1003	23.5	566.673	395.984	69.879
4:00 PM	50.4	1003	21.9	464.783	307.520	66.164
4:30 PM	48.24	1003	13.3	342.658	178.755	52.167
5:00 PM	25.92	1003	11.5	141.769	83.048	58.580

Table A2: Solar air heater performance on natural convection of air without multi-pass on 15/05/2016.

Time	Mass flow rate	Cp	□□□□□□ rise of air	$Q_{incidented}$	Q_{useful}	η_i (Instantaneous efficiency)
	kg/hr	J/Kg.k	K	(Watts)	$m*c_p$□□□	%
10:00 AM	50.4	1005	25.6	762.607	360.192	47.232
10:30 AM	67.68	1005	26.1	835.886	493.1334	58.995
11:00 AM	70.56	1005	26.3	894.751	518.0574	57.900
11:30 AM	69.12	1005	28.4	927.543	548.0064	59.081
12:00 PM	79.2	1005	26.2	956.446	579.282	60.566
12:30 PM	86.4	1005	28.3	941.586	682.596	72.494
1:00 PM	93.6	1005	24.9	933.181	650.637	69.722
1:30 PM	100.8	1005	22.4	867.720	630.336	72.643
2:00 PM	72	1005	24.8	820.611	498.48	60.745
2:30 PM	69.12	1005	20.6	730.784	397.4976	54.393
3:00 PM	67.68	1005	18	647.265	340.092	52.543
3:30 PM	64.8	1005	15	551.241	271.35	49.225
4:00 PM	61.2	1005	12.5	439.663	213.5625	48.574
4:30 PM	53.28	1005	9	327.532	133.866	40.871
5:00 PM	36.72	1005	9	218.067	92.259	42.308

Table A3: Solar air heater performance on natural convection of air with multi-pass of air on 05/06/2016.

Time	Mass Flow rate	Cp	□□□□□□ □ rise of air	$Q_{incidented}$	Q_{useful}	η_i (Instantaneous efficiency)
	kg/hr	J/Kg.k	K	(Watts)	$m*c_p$□□□	%
10:00 AM	51.84	1005	21.5	635.055	311.148	48.995
10:30 AM	53.28	1005	31.9	705.243	474.4806	67.279
11:00 AM	51.12	1005	31.5	786.110	449.5365	57.185
11:30 AM	58.32	1005	32.3	822.349	525.8763	63.948
12:00 PM	57.6	1005	34.8	813.826	559.584	68.760
12:30 PM	65.52	1005	32.6	823.350	596.2866	72.422
01:00 PM	64.08	1005	30.9	788.889	552.7701	70.069
01:30 PM	69.12	1005	24.1	747.030	465.0336	62.251
02:00 PM	79.2	1005	23.4	720.124	517.374	71.845
02:30 PM	69.12	1005	21.6	588.542	416.7936	70.818
03:00 PM	59.76	1005	17.2	422.549	286.9476	67.909
03:30 PM	79.2	1005	11.8	492.792	260.898	52.943
04:00 PM	60.48	1005	11	321.539	185.724	57.761
04:30 PM	46.08	1005	10.8	282.495	138.9312	49.180
05:00 PM	33.12	1005	8	125.480	73.968	58.948

Table A4: Solar air heater performance on natural convection of air with multi-pass of air on 27/06/2016.

Time	Mass Flow rate	Cp	□□□□□□ □ rise of air	$Q_{incidented}$	Q_{useful}	¦ $_i$ (Instantaneous efficiency)
	kg/hr	J/Kg.k	K	(Watts)	$m*c_p$□□□	%
10:00 AM	50.4	1005	21.8	748.027	306.726	41.005
10:30 AM	67.68	1005	26.6	824.318	502.5804	60.969
11:00 AM	70.56	1005	30.4	905.993	598.8192	66.095
11:30 AM	69.12	1005	30	952.592	578.88	60.769
12:00 PM	79.2	1005	31	968.741	685.41	70.753
12:30 PM	86.4	1005	29.3	959.956	706.716	73.620
01:00 PM	93.6	1005	25.5	929.917	666.315	71.653
01:30 PM	100.8	1005	21.9	910.011	616.266	67.721
02:00 PM	86.4	1005	24.4	825.619	588.528	71.283
02:30 PM	69.12	1005	23.8	747.203	459.2448	61.462
03:00 PM	67.68	1005	21.2	672.795	400.5528	59.536
03:30 PM	64.8	1005	18.1	566.674	327.429	57.781
04:00 PM	57.6	1005	13.84	464.784	222.5472	47.882
04:30 PM	43.2	1005	11.8	342.658	142.308	41.531
05:00 PM	18	1005	11.1	141.769	55.7775	39.344

Table A5: Solar air heater performance on Forced convection of air with multi-pass of air on 08/06/2016.

Time	Mass Flow rate	Cp	□□□□□□ □ rise of air	$Q_{incidented}$	Q_{useful}	¦ $_i$ (Instantaneous efficiency)	Thermo-hydraulic
	kg/hr	J/Kg.k	K	(Watts)	$m*c_p$□□□ (Watts)	%	Efficiency (%)
10:00 AM	36.144	1005	11.5	639.844	116.0373	18.135	17.198
10:30 AM	36.144	1005	14.1	724.342	142.27182	19.642	18.813
11:00 AM	36.144	1005	15	769.528	151.353	19.668	18.889
11:30 AM	36.144	1005	18.7	847.559	188.68674	22.262	21.554
12:00 AM	36.144	1005	16.6	855.481	167.49732	19.579	18.878
12:30 PM	36.144	1005	17.1	847.579	172.54242	20.357	19.649
01:00 PM	36.144	1005	18.8	788.126	189.69576	24.069	23.308
01:30 PM	36.144	1005	18.2	769.146	183.64164	23.876	23.096
02:00 PM	36.144	1005	22.6	721.423	228.03852	31.610	30.778
02:30 PM	36.144	1005	23.2	669.185	234.09264	34.982	34.085
03:00 PM	36.144	1005	19.4	569.987	195.74988	34.343	33.290

Table A6: Solar air heater performance on Forced convection of air with multi-pass of air on 09/06/2016.

Time	Mass Flow rate	Cp	□□□□□□ □ rise of air	$Q_{incidented}$	Q_{useful}	η_i (Instantaneous efficiency)	Thermo-hydraulic
	kg/hr	J/Kg.k	K	(Watts)	$m*c_p$□□□	%	Efficiency (%)
10:00 AM	54.216	1005	12.7	623.181	192.218	30.845	29.561
10:30 AM	54.216	1005	12.9	703.721	195.245	27.745	26.608
11:00 AM	54.216	1005	14	737.879	211.894	28.717	27.632
11:30 AM	54.216	1005	15.2	760.427	230.057	30.254	29.202
12:00 PM	54.216	1005	23.1	780.257	349.625	44.809	43.784
12:30 PM	54.216	1005	26.7	781.308	404.113	51.723	50.699
01:00 PM	54.216	1005	29.7	760.575	449.518	59.102	58.051
01:30 PM	54.216	1005	30.3	732.228	458.600	62.631	61.538
02:00 PM	54.216	1005	23.5	685.836	355.680	51.861	50.694
02:30 PM	54.216	1005	25.4	612.777	384.437	62.737	61.431
03:00 PM	54.216	1005	19.4	528.256	293.625	55.584	54.069

Table A7: Solar air heater performance on Forced convection of air with multi-pass of air on 09/06/2016.

Time	Mass Flow rate	Cp	□□□□□□ □ rise of air	$Q_{incidented}$	Q_{useful}	η_i (Instantaneous efficiency)	Thermo-hydraulic
	kg/hr	J/Kg.k	K	(Watts)	$m*c_p$□□□	%	Efficiency (%)
10:00 AM	72.288	1005	18.1	683.561	365.265	53.436	51.973
10:30 AM	72.288	1005	20.3	783.548	409.662	52.283	51.007
11:00 AM	72.288	1005	22.9	803.649	462.131	57.504	56.260
11:30 AM	72.288	1005	23.2	845.062	468.185	55.402	54.219
12:00 PM	72.288	1005	22.3	846.132	450.023	53.186	52.004
12:30 PM	72.288	1005	23.2	890.463	468.185	52.578	51.455
01:00 PM	72.288	1005	18	880.530	363.247	41.253	40.118
01:30 PM	72.288	1005	16.6	824.446	334.995	40.633	39.420
02:00 PM	72.288	1005	13.3	743.349	268.399	36.107	34.762
02:30 PM	72.288	1005	14	698.739	282.526	40.434	39.002
03:00 PM	72.288	1005	13.8	625.929	278.490	44.492	42.895

Table A8: Solar air heater performance on Forced convection of air with multi-pass of air with induced turbulence on 12/06/2016.

Time	Mass Flow rate	Cp	□□□□□□ □ rise of air	$Q_{incidented}$	Q_{useful}	¦ $_i$ (Instantaneous efficiency)	Thermo-hydraulic efficiency
	kg/hr	J/Kg.k	K	(Watts)	m*c_p□□□	%	Efficiency (%)
10:00 AM	36.144	1005	23.5	758.809	237.1197	31.249	29.799
10:30 AM	36.144	1005	24.5	851.469	247.2099	29.033	27.741
11:00 AM	36.144	1005	24.6	893.154	248.2189	27.791	26.560
11:30 AM	36.144	1005	27.3	931.496	275.4624	29.572	28.391
12:00 PM	36.144	1005	28.4	962.703	286.5616	29.766	28.624
12:30 PM	36.144	1005	31.1	926.003	313.8052	33.888	32.700
01:00 PM	36.144	1005	26.9	949.284	271.4263	28.593	27.434
01:30 PM	36.144	1005	28.2	911.884	284.5436	31.204	29.998
02:00 PM	36.144	1005	30.6	847.288	308.7601	36.441	35.143
02:30 PM	36.144	1005	31.4	768.707	316.8322	41.216	39.785
03:00 PM	36.144	1005	28.2	661.343	284.5436	43.025	41.362

Table A9: Solar air heater performance on Forced convection of air with multi-pass of air with induced turbulence on 14/06/2016.

Time	Mass Flow rate	Cp	□□□□□□ □ rise of air	$Q_{incidented}$	Q_{useful}	¦ $_i$ (Instantaneous efficiency)	Thermo-hydraulic
	kg/hr	J/Kg.k	K	(Watts)	m*c_p□□□	%	Efficiency (%)
10:00 AM	72.288	1005	19.8	634.985	399.572	62.926	60.879
10:30 AM	72.288	1005	23.7	705.243	478.275	67.817	65.974
11:00 AM	72.288	1005	24	786.110	484.330	61.611	59.957
11:30 AM	72.288	1005	27.4	822.349	552.943	67.239	65.659
12:00 PM	72.288	1005	23.1	813.826	466.167	57.281	55.684
12:30 PM	72.288	1005	23.6	823.350	476.257	57.844	56.265
01:00 PM	72.288	1005	23.1	788.889	466.167	59.092	57.444
01:30 PM	72.288	1005	23.3	747.030	470.203	62.943	61.203
02:00 PM	72.288	1005	24.3	720.124	490.384	68.097	66.292
02:30 PM	72.288	1005	20.1	588.542	405.626	68.921	66.712
03:00 PM	72.288	1005	13.2	422.549	266.381	63.042	59.965